Title

Growth factor—dependent phosphorylation of Gαi shapes canonical signaling by G protein—coupled receptors

Journal

Science Signaling, 17(839)

ISSN

1945-0877

Authors

Roy, Suchismita

Sinha, Saptarshi

Silas, Ananta James

et al.

Publication Date

2024-06-04

DOI

10.1126/scisignal.ade8041

Peer reviewed

HHS Public Access

Author manuscript

Sci Signal. Author manuscript; available in PMC 2024 August 16.

Published in final edited form as:

Sci Signal. 2024 June 04; 17(839): eade8041. doi:10.1126/scisignal.ade8041.

Growth factor–dependent phosphorylation of $G\alpha_i$ shapes canonical signaling by G protein–coupled receptors

Suchismita Roy[1], **Saptarshi Sinha**[1], **Ananta James Silas**[1], **Majid Ghassemian**[2], **Irina Kufareva**[3,*], **Pradipta Ghosh**[1,4,5,*,3]

[1]Department of Cellular and Molecular Medicine, University of California San Diego, CA 92093, USA.

[2]Department of Chemistry and Biochemistry, Biomolecular and Proteomics Mass Spectrometry Facility, University of California San Diego, San Diego, CA 92093, USA.

[3]Skaggs School of Pharmacy and Pharmaceutical Sciences, University of California San Diego, CA 92093, USA.

[4]Department of Medicine, University of California San Diego, CA 92093, USA.

[5]Moore's Comprehensive Cancer Center, University of California San Diego, CA 92093, USA.

Abstract

A long-standing question in the field of signal transduction is how distinct signaling pathways interact with each other to control cell behavior. Growth factor receptors and G protein–coupled receptors (GPCRs) are the two major signaling hubs in eukaryotes whose independent signaling mechanisms have been extensively characterized. We investigated how they may cross talk with each other. With linear ion trap mass spectrometry and cell-based biophysical, biochemical, and phenotypic assays, we found at least three distinct ways in which epidermal growth factor (EGF) affected canonical G protein signaling by the $G\alpha_i$ -coupled GPCR CXCR4 through the phosphorylation of $G\alpha_{i3}$. Phosphomimicking mutations in two residues in the αE helix of $G\alpha_i$ (Tyr^{154}/Tyr^{155}) suppressed agonist-induced $G\alpha_{i3}$ activation while promoting constitutive $G\beta\gamma$ signaling. Phosphomimicking mutations in the P-loop (Ser^{44}, Ser^{47}, Thr^{48}) suppressed G_i activation entirely, thus completely segregating growth factor and GPCR pathways. As expected, most of the phosphorylation events appeared to affect intrinsic properties of $G\alpha_i$ proteins, including conformational stability, nucleotide binding, and the ability to associate with and to release $G\beta\gamma$. However, one phosphomimicking mutation, targeting the C-terminal residue Tyr^{320}, promoted mislocalization of $G\alpha_i$ from the plasma membrane, a previously uncharacterized mechanism of suppressing GPCR signaling through G protein subcellular compartmentalization. Together, these findings elucidate not only how growth factor and chemokine signals crosstalk

*Corresponding author. ikufareva@ucsd.edu (I.K.); prghosh@ucsd.edu (P.G.).

Author contributions: I.K. and P.G. conceptualized the project; S.R., with assistance from A.S., performed experiments; I.K. performed all the computational analyses; M.G. and P.G. performed the in cellulo phosphorylation and LC/MS studies; S.R., S.S., I.K., and P.G. prepared figures for data visualization; S.S. provided expertise in statistical analysis; S.R., I.K., and P.G. wrote the original draft of the manuscript. All authors provided input and edited and revised the manuscript. All co-authors approved the final version of the manuscript. I.K. and P.G. coordinated and supervised all parts of the project and administered the project.

Competing interests: The authors declare that they have no competing interests.

through the phosphorylation-dependent modulation of $G\alpha_i$, but also how such crosstalk may generate signal diversity.

Introduction

A cell perceives and calibrates its responses to external cues through a complex array of sensor proteins, commonly known as receptors, which transduce signals from the plasma membrane (PM) to the cell's interior through a cascade of downstream intermediates. Traditionally studied through reductionist approaches by dissecting a single cascade at a time, it is well-known that these distinct cascades crosstalk at multiple levels. Cross-talk between multiple cascades generates a complex larger network for information flow, integration, and diversification (through context, time, and space), all of which ultimately coordinately control cell fate (1–4).

In eukaryotes, two of the most widely studied signaling cascades are those that are initiated by the receptor tyrosine kinases (RTKs) and by the 7-transmembrane receptors coupled to heterotrimeric G proteins (G protein–coupled receptors; GPCRs) (5). Upon sensing specific growth factors, RTKs autophosphorylate their cytoplasmic tails. Subsequently, various adaptor proteins dock onto those phosphosites to propagate the signal to the cell's interior (6). Heterotrimeric (henceforth, trimeric) G proteins, on the other hand, serve as molecular switches, canonically acting downstream of GPCRs (7, 8). Agonist-bound GPCRs act as receptor guanine nucleotide exchange factors (GEFs) for trimeric G proteins, stimulating GDP to GTP exchange on the Gα subunit and releasing Gβγ dimers. GTP-bound Gα monomers and Gβγ dimers bind to their effector molecules and transduce various signals (7).

Although it has been suggested that these two pathways crosstalk (9–13), in that G proteins may be activated downstream of RTKs (14–24), whether and how these processes take place in cells or how biologically important they are, still remain ambiguous. Reports as early as the late 1980s and early 1990s suggested that tyrosine-phosphorylation of G proteins is one such mechanism (25–28); however, the identities of these sites and how they might affect G protein activity remained unknown. In 2020, Kalogriopoulos *et al.* (5), showed that multiple RTKs (but not non-RTKs) can directly phosphorylate and transactivate the α-subunit of the trimeric Gi protein, that this phenomenon is mediated by scaffolding of monomeric $G\alpha_i$ with RTKs through the multimodular signal transducer, GIV (also known as Girdin) (29–31), and that the phosphorylation occurs on two tyrosines located within the inter-domain cleft of $G\alpha_i$ and one tyrosine located in the last β-strand (β6) (5). Phosphorylation activates $G\alpha_i$ by increasing the basal rate of GDP-to-GTP exchange and enhances its ability to suppress generation of the cellular second messenger cAMP. These insights defined a tyrosine-based G protein signaling paradigm and revealed its importance in eukaryotes; they also raised at least two important questions. First, given the plethora of kinases that are activated upon growth factor stimulation (not just TKs), what other sites may be phosphorylated and how might they (alone or in combination) affect $G\alpha_i$ activation? Second, how might these phosphorylation events affect the ability of canonical GPCRs to transduce signals through Gi? Furthermore, although growth factors, including epidermal growth factor (EGF)

and insulin-like growth factor-1 (IGF-1) inhibit Gi coupling to and activation by GPCRs (CXCR4) (26, 32), mechanisms for such uncoupling and deactivation remain elusive.

Here, we addressed these outstanding questions by interrogating how one prototypical growth factor–RTK system, the EGF–EGF receptor (EGFR) system, may shape one canonical GiPCR system (the chemokine system, CXCL12-CXCR4) through the phosphorylation of Gαi. We found that the phosphorylation events (phosphoevents) inhibited different aspects of signaling and did so through various mechanisms, with the location of the phosphosites on the G protein being a key determinant of how such inhibition was orchestrated.

Results

Distinct sites on $G\alpha_i$ are phosphorylated in the presence of EGF

In a previous study (5), we demonstrated that $G\alpha_{i3}$ undergoes tyrosine phosphorylation upon growth factor stimulation. These experiments were conducted in the presence of sodium orthovanadate, a commonly used inhibitor of protein phosphatases (33). Here, to determine which additional residues on $G\alpha_i$ are phosphorylated in the presence of growth factors, we performed in-cell kinase assays under similar conditions, immunopurified FLAG-tagged $G\alpha_{i3}$ ($G\alpha_{i3}$-FLAG) with an antibody against FLAG, and analyzed the immunoprecipitate by linear ion-trap mass spectrometry (MS) (34) (Fig. 1A; Materials and Methods). Before its use in these MS studies, we confirmed the functionality, localization, and EGF-dependent tyrosine-phosphorylation of the FLAG-tagged $G\alpha_i$ protein through a series of experiments addressing different aspects of $G\alpha_i$ function. In particular, we demonstrated that nonphosphorylated $G\alpha_{i3}$-FLAG bound to Gα-interacting protein (GAIP) (fig. S1A), a member of the regulator of G protein signaling (RGS) family, which serve as GTPase-activating proteins (GAPs) for $G\alpha_i$ (35), and that the EGF-dependent tyrosine-phosphorylation of $G\alpha_{i3}$-FLAG increased such binding. The C-terminal FLAG tag prevents $G\alpha_{i3}$-FLAG from coupling to intact GPCRs; however, we showed that both nonphosphorylated and tyrosine-phosphorylated $G\alpha_{i3}$-FLAG bound to the isolated third intercellular loop (icl3) of lysophosphatidic acid receptor 1 (LPAR1) and alpha 2A adrenergic receptors (α2A, B) (fig. S1B). The icl3 is a region that ensures the G protein–specificity of receptor GEFs (36). The ability of the nonphosphorylated and, to a lesser degree, the EGF-dependent tyrosine-phosphorylated form to bind to activator of G-protein signaling 3 (AGS3), a member of the GoLoco motif– [also known as the G protein regulatory (GPR) motif] containing proteins that act as guanine nucleotide dissociation inhibitors (GDIs) for $G\alpha_i$ (37, 38), was also demonstrated (fig. S1C). We also confirmed the unaltered ability of $G\alpha_{i3}$-FLAG to interact with Gβγ subunits in cells (fig. S1D) and bind to GIV, the prototypical member of the guanine nucleotide exchange modulators (GEM) (fig. S1E) (39, 40). These studies were performed with cells pretreated with orthovanadate in both stimulated and in serum-starved conditions, but robust tyrosine-phosphorylation of $G\alpha_{i3}$-FLAG was detected exclusively upon EGF stimulation (fig. S1, A to E), which suggested that it was growth factor–dependent. Finally, $G\alpha_{i3}$-FLAG localized prominently at the plasma membrane in serum-starved cells, with some diffuse cytosolic pattern observed upon EGF stimulation (fig. S1, F to I). The EGF-EGFR system was prioritized among other

growth factor systems for these studies, not only because EGFR is the prototypical growth factor RTK, but also because it is the most widely studied RTK for pathway crosstalk with GPCRs (41–43).

Two independent MS analyses were performed on the orthovanadate-pretreated, EGF-stimulated samples. Each time, the samples were processed without any phosphoenrichment to enable assessment of the relative stoichiometry of the various phosphosites. Different sets of phosphorylated peptides were identified (Fig. 1B), and seven sites were prioritized based on their confidence score, location within the G protein. and corroboration in independent LC/MS studies (Table 1). Projection of these residues on a topology map of $G\alpha_{i3}$ (Fig. 1C) and a solved crystal structure of the highly homologous $G\alpha_{i1}$ (Fig. 1D) revealed that the phosphorylated positions are located in some of the key regions within Gαi, spanning both the all-helical domain (AHD) and the Ras-like domain, the nucleotide-binding site, and the interdomain cleft. For example, Ser^{44}, Ser^{47}, and Thr^{48} are in the phosphate-coordinating P loop, Ser^{151} and Tyr^{154}/Tyr^{155} are in the αE helix, where they stabilize the αF helix and the conformational Switch-I (Sw-I), and Tyr^{320} is in the β6 strand, where it interacts with the C-terminal α5 helix directly engaging with activated GPCRs (44). Ser^{44}, Ser^{47}, Thr^{48}, and Tyr^{154} are strictly conserved across all mammalian Gα proteins, whereas Ser^{151} is replaced by asparagine and cysteine, and both Tyr^{155} and Tyr^{320} by phenylalanine in selected Gα protein subtypes (fig. S2). Apart from two characterized tyrosines (Tyr^{154} and Tyr^{155}) that are phosphorylated by RTKs within the interdomain cleft of $G\alpha_i$ (5), the other sites remain uncharacterized and their importance is unknown.

Previously, the roles of $G\alpha_i$ residues in the formation and stability of nucleotide-bound $G\alpha_i$ states or GPCR(rhodopsin)-$G\alpha_i$ complexes have been characterized comprehensively at a single amino-acid level by alanine scanning mutagenesis (44). A limited re-analysis of the dataset from Sun *et al.* (44), focused exclusively on the residues of interest in the current study, revealed that both of the P-loop residues Ser^{47} and Thr^{48} are critical for GTP binding, with Thr^{48} also being important for GDP binding, whereas mutations in Ser^{44} do not have much effect on either state (Fig. 1E, top). Alanine mutations of the interdomain cleft residues Ser^{151} and Tyr^{155} destabilized the GDP-bound state to a greater extent than the GTP-bound state, whereas elimination of Tyr^{154} did not have much effect on either state (Fig. 1E, top). The C-terminal residue Tyr^{320} was required for GPCR-$G\alpha_i$ complex formation and stability (Fig. 1E, bottom); however, alanine substitution at this site had only a moderate effect on the nucleotide-bound states (Fig. 1E, top) and no effect on heterotrimer formation (44). These findings suggest that phosphorylation at residues located in the P-loop and those buried within the interdomain cleft may primarily alter the kinetics of nucleotide exchange on the $G\alpha_i$ protein (and consequently its activity, conformation, and ability to sequester or release Gβγ), whereas phosphorylation at the C-terminal Tyr^{320} may primarily impair receptor engagement.

Finally, the distinct phosphosites identified in the presence of EGF were compared to phosphorylation events on $G\alpha_{i1}$, $G\alpha_{i2}$, and $G\alpha_{i3}$ previously detected by high-throughput MS (HTP-MS) (21, 23, 24, 26, 45, 46) [cataloged at phosphosite.org], and with previously reported sites of somatic mutations in cancer (cataloged in the COSMIC database). Such analysis showed that for four of seven phosphosites that we identified, the previously

reported phosphorylation events were induced by GPCR agonists (Table 1) and that other previously observed phosphorylation events and mutations tend to cluster in the same three regions of the $G\alpha_i$ protein: the P-loop, the interdomain cleft, and the C terminus, implying that these could represent “hot spots” within the allosteric switch (Fig. 1F).

Together, these data suggest that the seven prioritized $G\alpha_{i3}$ phosphorylation events (Fig. 1B, Table 1) are EGF-dependent, either based on their previously reported ligand-dependency (for Ser^{44}, Tyr^{154}, Tyr^{155}, and Tyr^{320}) or given their role in coordinating nucleotide binding in the dephosphorylated state (Ser^{47}, Thr^{48}, and Ser^{151}). We thus hypothesized that the $G\alpha_{i3}$ phosphorylation events that we observed in growth factor–stimulated cells may have interesting and meaningful consequences for canonical trimeric G protein signaling.

Study design and rationale

To study the effect of phosphorylation on G protein signaling, we resorted to the well-accepted norm of comparing the wild-type (WT) protein (which is expected to reversibly undergo cycles of phosphorylation and dephosphorylation as expected in physiologic state) against mutants with phosphomimicking and non-phosphorylatable substitutions that ‘“lock” the function of the protein in constitutively phosphorylated and dephosphorylated states, respectively. We generated phosphomimicking (Ser→Asp; Thr→Glu, and Tyr→Glu), and, in the case of Tyr^{320}, nonphosphorylatable (Tyr→Phe) mutants of these residues (table S1) based on the standard algorithm for residue-specific phosphorylation site replacements (47). Because alanine substitutions at the identified serine and threonine (but not the identified tyrosine) sites strongly affect the stability and properties of $G\alpha_i$ (Fig. 1E) (44), the use of Ser or Thr→Ala substitutions was deemed inappropriate; the inherent effect of such substitutions on protein stability was expected to confound any other effect of constitutive dephosphorylation in ways that would be impossible to interpret. Our decision to make them as single mutations, or as combinations, was guided by their location, concomitantly phosphorylated state in cells (Fig. 1B), and by theme, that is, pan-tyrosine, Tyr^{154}, Tyr^{155}, and Tyr^{320} combined or pan-pSerThr/Tyr, in which all sites identified and prioritized in this work were simultaneously substituted within the same construct (table S1). To enable functional characterization without the interference of endogenous G proteins, all mutations were generated in a $G\alpha_{i3}$ construct in which Cys^{351} was mutated to isoleucine. This C351I mutation renders the G protein insensitive to pertussis toxin (PTX) (48, 49) and enables, in conjunction with PTX treatment, to selectively assess the GPCR-related functions of the mutant G protein (50). Consequently, in all our assays, the PTX-sensitive, WT $G\alpha_{i3}$ (WTs) and the PTX-resistant $G\alpha_{i3}$ (WTr) served as negative and positive controls, respectively.

To assess the effects of the phosphomimicking $G\alpha_i$ mutations on the canonical signaling of Gi protein–coupled receptors (further abbreviated as GiPCRs), we used the prototypical family member, CXC chemokine receptor 4 (CXCR4), which couples to and transmits its signals primarily through PTX-sensitive Gi proteins (51). We chose CXCR4 because of the well-studied Gi-mediated signaling pathways that it activates in response to its endogenous agonist CXCL12 and because of its importance in cancer invasion and metastasis (51); the latter is a process that is enriched in pathway crosstalk between growth factors and GPCRs (41). In the case of CXCR4, previous studies have implied the presence of pathway crosstalk

with the EGF-EGFR pathway and the role of such crosstalk in promoting tumor progression (52, 53).

As a model system for our studies of $G\alpha_{i3}$ signaling downstream of CXCR4, we chose HeLa cells because of their abundance of endogenous CXCR4 (54) and their responsiveness to CXCL12 (54, 55). HeLa cells also known express a second receptor for CXCL12, ACKR3 (56–58); however, as an atypical chemokine receptor, ACKR3 exclusively transmits its signals through β-arrestin (56, 59–61) and therefore is unlikely to confound our assessment of $G\alpha_i$ mutant functionality.

Effects of the $G\alpha_i$ phosphomimicking mutations on canonical GiPCR-mediated $G\beta\gamma$ signaling

First, we assessed $G\beta\gamma$ release from the receptor-activated heterotrimeric $G\alpha_i$-$G\beta\gamma$ complex, which is one of the earliest steps and a key event in the transduction of GiPCR signals (62, 63). We assessed $G\beta\gamma$ release and activation by measuring agonist-induced changes in bioluminescence resonance energy transfer (BRET) between mVenus-tagged $G\beta\gamma$ (the BRET acceptor) and the RLuc8-tagged C-terminus of GPCR kinase 3 (GRK3ct, the BRET donor) (Fig. 2, A and B) (64–66). A CXCL12-induced increase in the BRET ratio indicates dissociation of the $G\alpha_i$-$G\beta\gamma$ heterotrimer and release of free $G\beta\gamma$, which then becomes available to interact with GRK3ct. Moreover, before CXCL12 stimulation, a higher basal BRET ratio between $G\beta\gamma$ and GRK3ct indicates basal excess of free (non-$G\alpha_i$-bound) $G\beta\gamma$ dimers, which is likely due to the compromised ability of mutant $G\alpha_i$ to sequester them and form stable $G\alpha i$-$G\beta\gamma$ heterotrimeric complexes.

After confirming that transfection of HeLa cells with various $G\alpha_i$ mutant constructs resulted in comparable amounts of exogenous protein (Fig. 2, C and D), we measured BRET in cells with or without PTX pretreatment and with or without CXCL12 stimulation. Before exposure to CXCL12, high $G\beta\gamma$-GRK3ct BRET was observed in the absence of exogenous $G\alpha_i$ (labeled “pcDNA”, 0% suppression of basal $G\beta\gamma$/GRK3ct association), this BRET was strongly suppressed when either WTs or WTr $G\alpha_{i3}$ was co-expressed (100% suppression of basal $G\beta\gamma$/GRK3ct association, Fig. 2, E and F), indicating the ability of both forms of $G\alpha_{i3}$ to bind to $G\beta\gamma$ and form stable heterotrimeric complexes, which was unaffected by PTX. In the assessment of CXCL12-induced increases in $G\beta\gamma$-GRK3ct association, as expected, WTs $G\alpha_{i3}$ was sensitive to PTX, whereas WTr $G\alpha_{i3}$ remained unaffected (fig. S3, A and B), indicating that the PTX-treated conditions are appropriate for drawing further conclusions regarding the effects of our mutant constructs without interference from endogenous $G\alpha_i$ proteins.

The three variants containing phosphomimicking mutations of Tyr^{154} and Tyr^{155} (YY154–155EE, YY154–155-320EEE, and pan-S/T/Y) demonstrated significant decreases in their ability to suppress the basal $G\beta\gamma$-GRK3ct BRET signal when compared to the positive control WTr, and no differences when compared to the negative control (pcDNA, no exogenous $G\alpha_i$) (Fig. 2, E and F, table S2), indicating that these mutants were impaired in $G\beta\gamma$ binding. These mutants also failed to show an increase in $G\beta\gamma$-GRK3ct association (indicative of $G\beta\gamma$ release from $G\alpha i$) upon ligand stimulation (Fig. 2, G and H, table S3), consistent with their inability to bind $G\beta\gamma$ in the first place. By contrast, the P-loop mutants

were either proficient (S44D) or partially proficient (S47D-T48E) in Gβγ sequestration under basal conditions; however, they were still defective in Gβγ release upon ligand stimulation (Fig. 2E). This may be a consequence of the inability of these mutants to bind GTP. Agonist-induced Gβγ release requires that $G\alpha_i$ is GTP-bound, but for at least two other substitutions at position 47 of $G\alpha_i$ (alanine and asparagine), a substantial impairment in GTP binding has been reported (44, 67), with the S47N mutant preferentially stabilizing (or trapping) a nucleotide-free, GPCR-bound state of the $G\alpha_i$-Gβγ heterotrimer (67–69). Additionally, an alanine substitution at position 48 abrogates the binding of both GDP and GTP (62). As for the C-terminal phosphosite Tyr^{320}, the phosphomimic Y320E substitution was partially deficient in Gβγ sequestration and incapable of Gβγ release after ligand stimulation. By contrast, the Y320F mutant was fully and partially proficient in Gβγ sequestration and release, respectively, suggesting that phosphorylation of $G\alpha_i$ at Tyr^{320} may be sufficient to inhibit canonical Gi signaling. Furthermore, although both the double YY154–155EE mutation and the triple YYY154–155-320EEE mutation completely abolished basal Gβγ sequestration (Fig. 2F) and ligand-stimulated Gβγ release (Fig. 2H), the replacement of Tyr^{320} with the non-phosphorylatable residue phenylalanine generated a mutant (YYY154–155-320EEF) that regained full proficiency in both Gβγ sequestration and partial proficiency in ligand-stimulated Gβγ release (Fig. 2, F and H). This indicates that the Y320F mutation rescued the defects observed in the double Tyr→Glu mutant within the interdomain cleft (tables S2 and S3; table S8).

These findings suggest that the $G\alpha_i$ phosphorylations that we observed in growth factor–stimulated cells can modulate canonical Gβγ signaling in at least two ways. First, they can impair the ability of the $G\alpha_i$ to form trimers with Gβγ under basal conditions, and consequently, inhibit canonical, ligand-dependent signaling while enabling constitutive activation of Gβγ (as exemplified by the phosphomimicking mutations at the interdomain cleft and at the C terminus). Second, they can inhibit ligand-stimulated Gβγ release but preserve, partially or fully, the ability to sequester Gβγ and form trimers under basal conditions (such as Ser/Thr phosphorylation in the P-loop). The mutation mimicking pan-phosphorylation at all serine, threonine, and tyrosine sites followed the first pattern. Furthermore, phosphorylation at Tyr^{320} (mimicked by the glutamine mutation) was sufficient to inhibit signaling, regardless of whether it was assessed independently by comparing the Y320E and Y320F mutants (tables S2 and S3) or in combination with other phosphotyrosines by comparing the YYY154–155-320EEE and YYY154–155-320EEF mutants (tables S2 and S3; table S8). In addition, the non-phosphorylatable Y320F mutant appeared to rescue the defects caused by the double YY154–155EE mutation.

Effects of the $G\alpha_i$ phosphomimicking mutations on canonical GiPCR-dependent inhibition of cAMP generation

As a G_i-coupled receptor, CXCR4 inhibits adenylyl cyclase (AC) activity, resulting in decreased amounts of intracellular cAMP (70). We investigated what, if any, effects the $G\alpha_i$ phosphomodifications had on this key step in chemokine receptor signaling. To this end, we used the established BRET-based sensor for cAMP, CAMYEL (cAMP sensor using YFP-Epac-RLuc), which monitors intracellular concentrations of cAMP in real time in live cells (Fig. 3, A and B) (71). By the design of the sensor, a decrease in the BRET

ratio (acceptor emission divided by donor emission) corresponds to an increase in cAMP concentration; therefore, for an intuitive display (fig. S4B), we expressed the results of this assay as inverse BRET (donor emission divided by acceptor emission); this quantity was further converted into suppression of cAMP generation (fig. S4A and Fig. 3, C and D). The abundance of cAMP was assessed after the addition of forskolin (FSK, a stimulator of AC) to cells pretreated with or without PTX and stimulated with or without CXCL12 (Fig. 3B; Materials and Methods). Basal or CXCL12-dependent suppression of FSK-induced cAMP generation were computed as percentages compared to the negative control (the WT PTX-sensitive $G\alpha_{i3}$, WTs) set at 0% and the positive control (the PTX-resistant $G\alpha_{i3}$, WTr) set at 100%. Compared to the positive control (WTr), none of the mutants significantly affected the basal suppression of FSK-induced cAMP generation (fig. S4A). In the context of chemokine-dependent suppression of cAMP generation, the P-loop (Ser^{47}/Thr^{48}), the β6-strand (Y320E), the pan-Y (YYY154–155-320EEE), and the pan-S/T/Y mutants were significantly different from the positive control and not different from the negative control (Fig. 3, C and D; fig. S4B; Table S4), indicating that these mutations abrogated the CXCL12-dependent suppression of cAMP generation through Gαi. This effect was similar to their impairment of ligand-induced Gβγ release. By contrast, the S151D and YYY154–155-320EEF mutants were no different from the positive control and significantly different from the negative control, indicating that they retained their ability to suppress cAMP generation. The rest of the mutants (S44D, YY154–155EE, and Y320F) were not significantly different from either the positive or negative control so that no conclusions could be made about their effects on the suppression of cAMP generation.

These findings suggest that some of the $G\alpha_i$ phosphorylation events that we observed in growth factor–treated cells can impair the ability of the $G\alpha_i$ to suppress cAMP generation downstream of agonist-activated GiPCRs, as exemplified by phosphorylation at Ser^{47} and Thr^{48} in the P-loop or the phosphorylation of Tyr^{320} in the C terminus. Other modifications are predicted to exert no effect, as exemplified by a selected phosphoserine-mimicking mutation in the interdomain cleft, Ser^{151}. Furthermore, the phosphomimicking mutation at Tyr^{320} (Y320E) was sufficient to inhibit signaling, whereas the combination of the nonphosphorylatable Y320F mutant with YY154–155EE did not appear to be significantly compromised (table S8).

Phosphomimicking and nonphosphorylatable mutations at Tyr^{320} affect the recruitment of $G\alpha_i$ to the receptor

The observed substantial and distinct effects of the phosphomimicking mutation Y320E and then nonphosphorylatable mutation Y320F on canonical Ga_i signaling are consistent with the location of Tyr^{320} in the $G\alpha_i$ β6 strand, where it directly contacts the GiPCR and the receptor-engaging C-terminal α5 helix of $G\alpha_i$ (Fig. 4, A and B) (44, 72), the latter through both nonpolar interactions and hydrogen bonds. Thus, we investigated whether and how the Y320E and Y320F mutants affected coupling of $G\alpha_i$ to a GPCR. To assess receptor recruitment, we used a well-defined, BRET-based assay in which Venus-tagged engineered “mini” Gα proteins engage RLuc-tagged GPCRs (73). Mini Gα proteins lack the membrane anchors, the N-terminal Gβγ-binding surface, and the α-helical domain (AHD) of G protein α-subunits, and contain a nuclear export signal (NES) (73). Ligand-dependent coupling of

a miniGα to an Rluc3-tagged GPCR results in a higher BRET ratio (Fig. 4, C and D). For Gi-coupled GPCRs, the appropriate miniGα to use is miniGαs/i, a chimera between $G\alpha_s$ and $G\alpha_i$. We confirmed by sequence alignment that Tyr^{320} in $G\alpha_i$ is conserved in $G\alpha_s$, and that the engineered mini$G\alpha_{s/i}$ protein also contains a tyrosine at the corresponding position (Fig. 4B). The corresponding tyrosine in mini$G\alpha_{s/i}$ was then mutated to either the phosphomimicking residue glutamate (Y320E) or the nonphosphorylatable residue phenylalanine (Y320F). We used these mutants alongside WT mini$G\alpha_{s/i}$ in a BRET-based acceptor saturation experiment in which the amount of plasmid encoding the donor (CXCR4 C-terminally tagged with RLuc3) in the transfections was kept constant while the amount of the acceptor-encoding plasmid (Venus-tagged mini$G\alpha_{s/i}$-WT or the Y320E/F mutants) was titrated. The resulting normalized BRET ratio showed that, as expected, GPCR coupling upon ligand stimulation was saturated in the case of mini$G\alpha_{s/i}$-WT but was impaired in the case of the Y320E and Y320F mutants (, Fig. 4, E and F). Although the F-test showed no statistically significant difference between the Y320E and Y320F mutants, numerical fit parameters are consistent with the Y320E mutant being more compromised than the Y320F mutant (Fig. 4, E and F, table S5). This finding was consistent with observations across all tested acceptor transfection levels (fig. S5A) and was further confirmed through double-reciprocal (Lineweaver-Burk, LB) plot analysis (fig, S5, B and C, table S6) which indicated that mini-Gαs/i-Y320E was the most compromised and, as a result, did not conform to a one-site saturable binding model. Titration of the amount of BRET acceptor was verified by flow cytometry analysis (fig. S5, D to F).

These findings suggest that Tyr^{320} is a key determinant of GPCR coupling. We thus conclude that the corresponding phosphoevent at $G\alpha_{i3}$ Tyr^{320} (which we observed in EGF-treated cells) may be sufficient to uncouple the G protein from GiPCRs, which is consistent with a study showing that growth factor stimulation leads to the release of $G\alpha_i$ from CXCR4 (74). Because Tyr^{320} engages in (distinct) intramolecular H-bonds in both the inactive and GiPCR-activated conformations (Fig. 4A), the intermediate performance of the Y320F mutant in these receptor recruitment assays is not unexpected.

Effects of the phosphosites on canonical GPCR-stimulated chemotaxis

Next, we investigated whether the overall theme of phosphotyrosine-mediated inhibition of GPCR coupling (Tyr^{320}) and of canonical $G\alpha_i$-mediated inhibition of cAMP (Tyr^{320}) and $G\beta\gamma$ signaling ($Tyr^{154/155}$ and Tyr^{320}) was functionally relevant and resulted in phenotypic changes in cells. To this end, we assessed the effects of mutation of these three tyrosines on chemotaxis, because the CXCL12-CXCR4 axis stimulates chemotaxis in a Gαi-dependent manner (55). We used a transwell assay system in which HeLa cells migrated across a 0 to 40 nM CXCL12 gradient for 20 hours in the presence of PTX (Fig. 5A), a duration that was chosen based on a previous study (60). The positive and negative controls in our assay behaved as expected, that is, cells expressing the PTX-sensitive WTs G protein (negative control) did not migrate, whereas those expressing the PTX-resistant WTr G protein (positive control) migrated in the presence of PTX (Fig. 5B, top, and Fig. 5C). When compared to cells expressing the PTX-resistant WTr G protein, those expressing all but one of the mutants showed various degrees of impairment in their ability to chemotax (Fig. 5, B and C); cells expressing the YYY154–155-320EEF mutant performed just as

well as those expressing WTr. Cells expressing the YYY154–155-320EEF mutant migrated in greater numbers compared to those expressing the other mutants, including Y320E, YYY154–155-320EEE, and YY154–155EE (table S7). Cells expressing the Y320F mutant migrated in greater numbers compared to those expressing the Y320E mutant (table S7). These findings indicate that the Y320E mutation in Ga_{i3} was sufficient to inhibit CXCL12-stimulated chemotaxis and that the Y320F mutation was sufficient to reverse the inhibitory effects observed in tyrosine-to-glutamate mutations within the interdomain cleft.

Together, our results indicate that the $G\alpha_i$ phosphomodifications that we found in EGF-stimulated cells generally inhibited canonical, GPCR-driven chemotaxis, as exemplified by almost all the mutants. Consistent with all other readouts, the phosphomimicking mutation at Tyr^{320} was sufficient to inhibit chemotaxis, alone or in combination with YY154–155EE (table S8). However, as was seen in the $G\beta\gamma$ release and activation assays, the nonphosphorylatable Y320F mutation rescued the deficiencies of not only the triple phosphomimic, YYY154–155-320EEE, but also those of the double mutantion, YY154–155EE.

Structural analysis of the phosphomimicking and nonphosphorylatable $G\alpha_i$ mutations

To put these experimental findings into a structural context, we projected the mutated residues onto the $G\alpha_i$ structure in three structurally characterized functional states: the inactive, GDP-bound state with $G\beta\gamma$, the nucleotide-free state in complex with a GPCR and $G\beta\gamma$ (this transient state corresponds to nucleotide release); and an active, GTP-bound state (Fig. 6A). This analysis revealed the proximity and interactions of all three P-loop residues with the nucleotides, with Thr^{48} directly coordinating the first phosphate for both GDP and GTP, Ser^{47} the Mg^{2+} ion in the GTP-bound state, and Ser^{44} forming a hydrogen bonding network with Lys^{45} and the second phosphate of GDP or GTP. These observations suggest that phosphorylation (or phosphomimicking mutations) at these positions would disrupt the ability of $G\alpha_i$ to bind to nucleotides and hence participate in the GDP-GTP exchange cycle downstream of agonist-stimulated GiPCRs. In the nucleotide-free, GPCR-bound state, these residues do not form any critical contacts, which is why their mutation may trap this state, similar to dominant-negative $G\alpha_i$ (69).

The Ser^{151}/Tyr^{154}/Tyr^{155} cluster in the αE helix is engaged in a dense hydrogen-bonding network in both nucleotide-binding states, which is partially released in the domain-open, nucleotide-free state (Fig. 6A). Indeed, Tyr^{155} is fully buried in all of the structurally characterized states of Gαi, suggesting that for it to be phosphorylated, the AHD must partially unfold. Tyr^{154}, however, may become exposed through a rotamer change, especially in the nucleotide-free state.

Further observations are related to Tyr^{320} in the β6 strand. In the nucleotide-bound states, this residue packs against the receptor-engaging C-terminal α5 helix and forms a hydrogen bond with Asn^{346} (Fig. 6A). In the process of $G\alpha_i$ activation by the receptor, due to a rotation and an upward shift of the α5 helix, this residue switches its hydrogen bonding to Lys^{345} and Asp^{341}, while continuing to provide the stabilizing and packing interactions for that helix. In other words, Tyr^{320} works both as a stabilizing residue and a conformational switch in the process of $G\alpha_i$ activation by a GPCR. We hypothesize

that Tyr^{320} phosphorylation or its replacement by the phosphomimicking residue glutamate reduces the stability of the C-terminal α5 helix and may, for example, make it more prone to leaving its location in the center of the $G\alpha_i$ GTPase domain β-barrel (75, 76). In contrast, the Y320F mutation still enables this residue to serve its stabilizing role for the α5 helix, because only the hydrogen bond switching functionality is eliminated by that mutation.

Next, we computationally assessed the stabilities of the various structurally characterized functional states of $G\alpha_i$ when mutated at the phosphorylated positions. Four conformational states were assessed: the nucleotide-free state in complex with a GPCR and Gβγ; the GDP-bound state; the GTP-bound state with Gβγ; and the GTP-bound state, and multiple experimental structures were included where available. The effects of mutations on the stability of each state were calculated and expressed as the predicted ΔΔG of folding, with positive values indicating destabilization (state disfavored) and negative values indicating stabilization (state favored) (Fig. 6B and fig. S6).

The S44D and S151D mutations were predicted to slightly favor the nucleotide-free, receptor- and Gβγ-bound states. Consistent with previous studies (44, 69), the S47D mutation was predicted to strongly disfavor the GTP-bound state of Gαi, whereas the T48D mutation disfavors the GDP-bound state. The phosphomimicking mutations at Tyr^{154} and Tyr^{155} were predicted to be strongly destabilizing in general, with somewhat milder effects on nucleotide-free, receptor- and Gβγ-bound Gαi. Similarly, the Y320E mutation was strongly destabilizing, with the GDP- and Gβγ-bound state of $G\alpha_i$ most affected (fig. S6). In contrast, the Y320F mutation was predicted to have only a minor destabilizing effect, and the GDP-bound states were the least affected (Fig. 6B and fig. S6). Together, these structural and computational observations provide a rational basis for the experimentally observed effects of the mutations.

Effects of the phosphomimicking and nonphosphorylatable mutations on the membrane localization of $G\alpha_{i3}$

The contrasting effects of the phosphomimicking mutant Y320E (and YYY154–155-320EEE) and the nonphosphorylatable mutant Y320F (and YYY154–155-320EEF) across all readouts (table S8) led us to hypothesize that the Y320F mutation may provide an advantage that drives the observed proficiency of the G protein in most assays. Because all of the mutants were expressed at similar abundances in cells (Fig. 2, C and D), they were unlikely to differentially affect protein stability; thus, we investigated protein localization. Confocal immunofluorescence studies of HeLa cells revealed a substantial difference in the localization patterns (Fig. 7A). $G\alpha_i$ proteins with tyrosine or phenylalanine at position 320 (Y320F, YY154–155EE, and YYY154–155-320EEF) localized predominantly at the peripheral membrane, presumably the plasma membrane; however, proteins with a glutamate at that position (Y320E and YYY154–155-320EEE) localized predominantly in the cytosol. Furthermore, cell fractionation assays confirmed these findings. $G\alpha_i$ proteins with an intact Tyr^{320} (WTr or YY154–155EE mutant) or those in which Tyr^{320} was substituted with phenylalanine (EEF and Y320F mutants) were detected in the crude membrane fractions, indistinguishable from each other. However, the $G\alpha_i$ proteins in

which the Tyr^{320} was substituted with glutamate (Y320E and EEE mutants) were detected primarily in cytosolic fractions (Fig. 7, B and C).

These findings demonstrate that Tyr^{320} is a key determinant of the localization of $G\alpha_{i3}$. That the Y320E mutant localizes in the cytosol but Y320F localizes at the plasma membrane suggests that the EGF-dependent phosphorylation of Tyr^{320} may be sufficient for $G\alpha_i$ mislocalization. To test this, we used confocal microscopy to assess protein localization in cells with or without EGF stimulation (Fig. 7D). In serum-starved cells, WT $G\alpha_i$ localized to the plasma membrane (Fig. 7A) and in the perinuclear region, presumably at the Golgi (Fig. 7D), as shown previously (77). In response to EGF, the plasma membrane–localized pool was selectively lost. Such ligand-dependent changes in localization were abolished for the Y320E and Y320F mutants. Plasma membrane localization was undetectable in the case of the constitutive phosphomimic Y320E mutant (Fig. 7D) and stably detected for the nonphosphorylatable Y320F mutant (Fig. 7D) regardless of ligand stimulation. Furthermore, that the YY154–155EE and YYY154–155-320EEF mutants localized at the plasma membrane but that YYY154–155-320EEE localized to the cytosol (Fig. 7, C and D) indicates that phosphorylation at Tyr^{320} may be required for $G\alpha_{i3}$ to lose its plasma membrane localization (table S8).

Discussion

Canonical heterotrimeric G protein signaling is stimulated by ligand-activated GPCRs; however, the canonical GPCR pathways have been shown in many contexts to be subject to crosstalk and regulation by growth factors. Here, we revealed the molecular mechanisms that enable growth factor RTKs to modulate canonical G protein signaling. More specifically, we showed that growth factors may shape canonical signaling, in part, through the phosphorylation of $G\alpha_i$ (Fig. 8). Phosphorylation occurred at key residues located at three strategic hot spots within the GTPase: the P-loop, the interdomain cleft, and the C-terminus. Using a library of phosphomimicking mutants in a series of assays to interrogate some of the most upstream (receptor recruitment and trimer dissociation) and downstream (cAMP inhibition and chemotaxis) events in canonical GiPCR signaling, we showed that the phosphomodifications predominantly inhibited ligand-induced signaling, with some also promoting constitutive $G\beta\gamma$ signaling. These findings illuminate the basis for some poorly understood observations by others that growth factors (EGF and IGF1) inhibit Gi coupling to and activation by GPCRs (CXCR4) (32, 53, 74). Because phosphorylation of $G\alpha_i$ at Tyr^{154} and Tyr^{155} by RTKs, such as EGFR, increases its basal GDP-to-GTP exchange rate by ~15.6-fold (5), our findings imply that phosphomodulation of $G\alpha_i$ downstream of growth factors may serve as a key determinant of whether a G protein is activated by canonical vs. noncanonical, GPCR-independent mechanisms. Whereas physiologic growth factor signaling may spare the G protein for canonical signaling downstream of GPCRs, inappropriate signaling in pathologic conditions, such as cancer, may sequester the G protein from canonical GiPCR-dependent pathways (shown here), and instead, facilitate the transduction of noncanonical signals, as shown previously (5). Such sequestration may facilitate the contextualization of signals; for example, although phosphorylation of the interdomain tyrosines (Y^{154}/Y^{155}) could suppress cAMP generation upon growth factor stimulation and enhance migration during wound closure or invasion through matrix proteins

(5), such phosphorylation (mimicked by the YY154–155EE mutant) was unable to suppress cAMP generation or support chemotaxis upon GiPCR stimulation.

We showed three possible mechanisms for the inhibition of canonical signaling, dependent on the location of the phosphosites within the G protein (Fig. 8 and table S8). First, in application to key residues at the interdomain cleft, Ser^{151}, Tyr^{154} and Tyr^{155} (which are phosphorylated in combination with $pSer^{151}$ alone and pY^{154}/pY^{155}), our results suggest that whereas phosphorylation at Ser^{151} had little or no effect, phosphorylation at the pair of tyrosines impaired ligand-stimulated Gβγ release, partially impaired the ligand-stimulated suppression of cAMP generation, and inhibited chemotaxis. Furthermore, all of this occurred in the background of enhanced constitutive Gβγ signaling because of the impaired ability of the mutated/phosphorylated $G\alpha_i$ to bind, sequester, and inactivate Gβγ. Computational analyses suggest that both phosphorylation (5) and phosphomimicking mutations (shown here) at Tyr^{154} and Tyr^{155} favor the nucleotide-free state of Gαi. These findings are consistent with our previous work (using nonphosphorylatable mutants in FRET-based assays), which showed that dual phosphorylation at Tyr^{154} and Tyr^{155} is required for growth factor–stimulated dissociation of the heterotrimer and increases basal nucleotide exchange rate (~5-fold higher than that of the WT) (5). The increased basal activity was attributed to disrupted intermolecular interactions and packing (loss of H-bonds) within the inter-domain cleft, which may affect the opening and closing of the all-helical and Ras-like domains (5). Although molecular dynamic simulation studies showed that domain opening is insufficient for GDP release (78), phosphorylation at Tyr^{154} and Tyr^{155} may affect neighboring residues within the nucleotide-binding pocket, such as those in the αD to αE loop, which includes the so-called NDS^{151} motif. Alternatively, because both Tyr^{154} and Tyr^{155} face toward αF and Sw-I, particularly Tyr^{155}, it is possible that destabilization of Sw-I could serve as a mechanism for pTyr-induced allosteric enhancement of GDP release. Sw-I was identified as a key conduit in the allosteric path to nucleotide release that is triggered by the guanine-nucleotide exchange factor, GIV/Girdin, transmitting forces from Sw-II to the hydrophobic core of the GTPase (5). Although the identity of the kinase that phosphorylates Ser^{151} remains unknown, Tyr^{154} and Tyr^{155} are phosphorylated by multiple RTKs (but not by non-RTKs) (5). Regardless of which kinase phosphorylates these sites and how they affect the basal exchange rate, what is clear is that they functionally uncouple the G protein from GPCRs by reducing Gβγ-binding and trimer assembly. In doing so, the interdomain cleft events segregate the RTK-to-$G\alpha_i$ pathway (with resultant higher basal activity) from the canonical GPCR-to-$G\alpha_i$ pathway.

Second, our data indicate that the phosphorylation of key residues within the P-loop, Ser^{44}, Ser^{47}, and Thr^{48} (the latter two are simultaneously phosphorylated), impairs ligand-stimulated Gβγ release and prevents suppression of cAMP generation, but largely spares the ability of $G\alpha_{i3}$ to bind to Gβγ and assemble heterotrimers. Computational analyses revealed that a phosphomimic at Ser^{47} preferentially destabilizes the GTP-bound state, whereas a phosphomimic at Thr^{48} destabilizes the GDP-Gβγ-bound Gαi. These findings are not unexpected, because the P-loop, which is essentially the sequence ^{40}GAGESGKST^{48} (79), participates in nucleotide binding and coordination of Mg^{2+} (80); whereas Ser^{47} coordinates the Mg^{2+}, Thr^{48} bridges the β and γ phosphates in GTP. Our findings are consistent with previous work suggesting that phosphorylation at Ser^{44} on $G\alpha_{i2}$ was a basis

for the desensitization of μ-opioid receptors (81). Similarly, the S47R mutant $G\alpha_{i3}$, which is implicated in auriculo-condylar syndrome (ACS), is a dominant-negative proteins that couples to GPCRs but cannot bind to or hydrolyze GTP (82). A similar effect was observed in the case of $G\alpha_q$ (Ser^{53}, which corresponds to Ser^{47} in Gαi); phosphorylation of this site impedes GTP-binding and downstream signaling events (83). Although the identity of the kinase(s) that phosphorylate these P-loop sites remains unknown, the phosphorylation functionally uncouples the G protein from GPCRs by reducing ligand-induced Gβγ release but without increasing the constitutive activity of Gβγ. Because coupling to Gβγ and the GPCR are unlikely to be affected, $G\alpha_i$ proteins phosphorylated at these sites may behave as dominant-negative proteins that couple to the GPCR but cannot release Gβγ, nor will they bind to and hydrolyze GTP. Thus, the P-loop sites may not only inhibit the canonical GPCR-to-$G\alpha_i$ pathway, but they have the potential to exert a dominant-negative effect.

Third, our data suggest that phosphorylation of Tyr^{320}, a key residue in the C-terminal β6 strand, impairs Gβγ-binding and ligand-stimulated Gβγ release, receptor coupling, and ligand-stimulated suppression of cAMP generation and inhibits chemotaxis. A previous study revealed the importance of this residue in coupling to GPCRs (44), and we previously established that Tyr^{320} is phosphorylated by RTKs, both in vitro and in cells (5). We found that the phosphomimicking mutation of Tyr^{320}, either alone or in combination with mutations of other tyrosines in the interdomain cleft, rendered the G protein inert in canonical signaling. Furthermore, the Y320F mutant $G\alpha_i$ not only retains the ability to bind to Gβγ, but also the ability of mediate ligand-stimulated Gβγ release, which is consistent with this residue being a phenylalanine in other G protein α-subunits, for example, $G\alpha_{15}$ and $G\alpha_{12}$ (fig. S2). Unexpectedly, Y320F mutant $G\alpha_{i3}$ reversed the defects in signaling observed for proteins in which the two tyrosines in the interdomain cleft region were phosphorylated. We hypothesize that this effect is primarily through restoring the ability of the mutant $G\alpha_i$ to bind to Gβγ and assemble heterotrimers (table S8). The Y320F mutation also reversed the effects of the Y320E mutation in pan-Tyr mutants, which we hypothesize is because of their contrasting patterns of protein localization: proteins with Y320E (alone or in combination with mutants of the interdomain cleft) were cytosolic, whereas proteins with Y320/Y320F (alone or in combination) were localized to the plasma membrane. As for the mechanism by which Tyr^{320} determines membrane localization, it is unlikely to be due to either of the two known determinants of membrane localization of $G\alpha_i$ subunits, that is, N-terminal myristoylation and palmitoylation and association with Gβγ dimers (17). The YY154–155EE mutant, which was deficient in Gβγ-binding, was localized to the plasma membrane. It was unclear how the Y320E mutation alone was sufficient to abrogate Gβγ-binding; however, structural insights into how the G protein chaperone and guanine nucleotide exchange factor Ric-8 binds to Ga_i (76) provided a potential explanation. The Gαi-Ric8 complex requires the β4 to β6 strands of Gαi, and Tyr^{320}(β6) serves as a contact site (76), which suggests that it may be a critical determinant of the interaction. Note that the Y320E $G\alpha_i$ mutants in our study mimicked the defects previously reported in Ric8-depleted diverse systems (fungi, flies, worms, and mammals), that is, $G\alpha_i$ subunits show reduced steady-state abundance and localization at the plasma membrane, associate inefficiently with Gβγ dimers, and consequently assemble heterotrimers poorly (75, 84–88). Whether phosphorylation of $G\alpha_i$ at Tyr^{320} affects its interaction with and modulation by

Ric8 remains to be explored. Regardless, our findings suggest that phosphorylation of $G\alpha_{i3}$ at Tyr^{320} in response to EGF impairs its GPCR coupling and plasma membrane localization and thereby inhibits signaling through the canonical GPCR-to-$G\alpha_i$ pathway.

Finally, note that in addition to modulating $G\alpha_i$, GIV also modulates $G\alpha_s$ (40), raising the possibility that GPCRs that couple to $G\alpha_s$ may also be similarly affected by EGFR-dependent phosphomodulation. We noted that although Ser^{44}, Ser^{47}, Thr^{48} and Tyr^{154} are conserved in $G\alpha_s$, Ser^{151} and Tyr^{155} are not (fig. S2). Although Tyr^{320} is conserved in $G\alpha_s$, the flanking sequence is not. Consistent with this, we previously showed that $G\alpha_i$, but not $G\alpha_s$, is a preferential substrate of EGFR (5). In contrast, we found that Src phosphorylated all of the G proteins tested equally efficiently, including $G\alpha_s$ and $G\alpha_i$ (5).

In terms of the limitations of our study, we did not evaluate the myriad downstream signaling pathways that are stimulated by CXCL12, which must be investigated to assess the full effects of the phosphomodifications we have characterized. Neither did we reveal the identity of the serine and threonine kinases that mediated the EGF-dependent phosphorylation of $G\alpha_{i3}$. It is possible that the phosphoevents that we report here exert their effects either independently of each other or influence each other (perhaps resulting in some logical sequence or hierarchy). Although these aspects remain unknown, any phosphosite that accelerates nucleotide exchange can be expected to enhance the phosphorylation of residues that are buried within the interdomain cleft and hence, are otherwise inaccessible to kinases. Although we expect that our findings are likely relevant across other cell types, it is possible that our findings in HeLa cells may be uniquely affected by the endogenous abundance of $G\beta\gamma$ subunits and AC isoforms.

In conclusion, we showed how the diverse $G\alpha_i$ phosphoevents that were observed in EGF-stimulated cells exerted a coherent effect, that is, they all inhibited canonical GPCR signaling through distinct mechanisms that correlated with the locations of the phosphosites. Together, these findings provide mechanistic insights into how growth factors inhibit canonical GPCR-dependent G protein signaling.

Materials and Methods

Regents and consumables

All of the regents, consumables, and software programs used in this work are listed in table S9.

Constructs and cloning

The cDNA encoding wild-type (WT) rat $G\alpha_{i3}$, obtained from A. Spiegel (National Institutes of Health, Bethesda, MD), was subcloned into pcDNA 3.1 and validated previously (89). Using this construct as template, we generated all of the other $G\alpha_{i3}$ mutants used in this study with a QuikChange Site-Directed Mutagenesis Kit (Stratagene) as per the manufacturer's protocol. A variant that is insensitive to ADP-ribosylation by *Bordetella pertussis* toxin (PTX) (48) was generated for each construct by mutating Cys^{351} into isoleucine (90). A BRET-based CAMYEL sensor [cAMP sensor using YFP-Epac-RLuc (71)] was a gift from P. Insel and T. Handel (University of California, San Diego). V2-

CAMYEL, a modified version of the sensor with increased luminescence, was generated by site-directed mutagenesis of the RLuc region (C124A/M185V) (91). Recombinant CXCL12 was expressed and purified exactly as described previously (92). Both mVenus-hGBB1 and mVenus-hGBG2 were a gift from N. Lambert, Augusta University (93). The mini-$G\alpha_i$ construct was a gift from N. Lambert. The mini-$G\alpha_{s/i}$ construct is a chimera of $G\alpha_s$ and $G\alpha_i$, keeping in parity the Tyr^{320} residue of $G\alpha_{i3}$ and $G\alpha_s$, and the Y320E and Y320F mutants were generated with a QuikChange Site-Directed Mutagenesis Kit.

Pulldown and immunoprecipitation assays

These studies were performed as described previously (39, 94–96). For in vitro pull-down assays, COS7 cells expressing $G\alpha_{i3}$-FLAG and other required constructs were serum-starved for ~16 to 18 hours, pre-incubated with 100 μM sodium orthovanadate for 1 hour, left unstimulated or stimulated with 50 nM EGF for 15 min, and lysed on plate in lysis buffer [25 mM HEPES (pH 7.4), 100 mM NaCl, 10 mM MgCl2, 30 μM GDP, 2 mM DTT, 0.5% Triton X-100, 1x Complete Protease Inhibitor Mixture (Roche), and 1× Sigma Phosphatase Inhibitor cocktails 1 and 2 (Cat# P2850 and #P5726; Sigma)]. Equimolar amounts of bacterially expressed and purified GST-tagged proteins or GST alone (as a negative control) immobilized on glutathione-Sepharose beads were incubated with pre-cleared COS7 cell lysates in the same lysis buffer. Bead-bound proteins and lysates were incubated with constant tumbling at 4°C for 4 hours. The beads were washed four times with 1 ml of lysis buffer and were eluted in 1× Laemmli sample buffer by heating to 95°C for 5 min. Eluates were then resolved by SDS-PAGE, transferred to a PVDF membrane, and incubated with the appropriate antibodies. Bound total and phosphorylated $G\alpha_{i3}$-FLAG were analyzed by dual-color Western blotting. In the case of His-GIV-CTs pulldown studies, the protein was bound to HisPur Ni-NTA Resin (Thermo Fisher) and the remaining steps were performed as described for the pulldown assays with GST proteins. For immunoprecipitation studies with endogenous $G\beta\gamma$, equal aliquots of lysates (~2 mg of total protein prepared exactly as described earlier) of serum-starved or EGF-stimulated cells, transfected (or not) with plasmid encoding FLAG-tagged $G\alpha_{i3}$, were incubated for 3 hours at 4°C with 2 μg of anti-FLAG mAb. Protein G Sepharose beads were added and incubated at 4°C for an additional 60 min. Beads were washed and bound immune complexes were eluted by boiling in Laemmli's sample buffer.

In cellulo phosphorylation of $G\alpha_{i3}$ protein and linear ion trap mass spectrometry

COS7 cells were cultured according to American Type Culture Collection (ATCC) guidelines. To analyze $G\alpha_{i3}$ phosphorylation, COS7 cells were transiently transfected with plasmid encoding WT $G\alpha_{i3}$ C-terminally tagged with the FLAG tag and serum-starved for 16 hours (0 % FBS) before stimulation with 50 nM EGF for 15 min in the presence of the cell-permeable tyrosine phosphatase inhibitor, sodium orthovanadate (100 μM, added 1 hour before the EGF). Reactions were stopped with PBS chilled to 4ºC and supplemented with 200 μM sodium orthovanadate and serine and threonine phosphatase inhibitor (Sigma), after which the cells were immediately scraped and lysed. Cell lysates for MS analysis were prepared by resuspending cells in lysis buffer [20 mM HEPES, (pH 7.2), 5 mM magnesium acetate, 125 mM potassium acetate, 0.4% Triton X-100, 1 mM DTT, supplemented with sodium orthovanadate (500 μM), phosphatase (Cat# P0044; Sigma) and protease (Roche)

inhibitor cocktails], after which they were passed through a 28G needle at 4°C, and cleared by centrifugation at 10,000g for 10 min before use in subsequent experiments. Equal aliquots of lysates were used as a starting material for the immunoprecipitation of $G\alpha_i$ with an antibody that recognizes the FLAG tag (Sigma) together with protein G beads. To determine the phosphorylation states of FLAG-$G\alpha_{i3}$, we used the QTRAP 5500 in the selected reaction monitoring (SRM) mode to scan for all possible phosphorylated forms (phosphoforms) of the protein. For this purpose, the bead-antibody-protein complex was trypsinized in solution with the aid of Rapigest surfactant and analyzed by six distinct tandem mass spectrometry acquisition methods using a quadrupole time of flight (QSTAR Elite ABSCIEX) instrument and the ABSCIEX QTRAP 5500 hybrid mass spectrometer. The acquisition methods were as follows. First, the data-dependent MS2 method with the QSTAR Elite. Second, the data-dependent MS2 method with the QTRAP 5500. Third, multiple reaction monitoring (MRM) methods for all possible phosphoforms of the target protein with the QTRAP 5500 (data file S1). Fourth, MRM-triggered full-scan MS2 methods for the detected peptide phosphoforms with the QTRAP 5500 in the trap mode. Fifth and sixth, precursor ion scans for −79 (in negative ion mode for S/T[P]) and 216.04 (in positive ion mode for Y[P]) ions. Upon detection of these indicator ions, the mass spectrometer switches to ion trap mode to collect the MS2 spectrum. SRM methods were developed for all possible tryptic peptides in phosphorylated and nonphosphorylated states. The ABSCIEX SRM Pilot software was used for SRM method development. Ultimately, a method with 210 SRM transitions states was developed for the phosphorylated and nonphosphorylated tryptic peptides of $G\alpha_{i3}$. In most cases, there were at least two transitional states used for a given peptide mass. A total of 13 unique phosphorylation sites in the $G\alpha_{i3}$ protein were detected with the QTRAP 5500, of which three were tyrosines (data file S2). Because the samples were not subjected to phosphoenrichment before the MS analyses were performed, the stoichiometry of any phosphoevent was calculated based on the ration of phosphorylated to total peptides of any given sequence (data file S1). Another aliquot (10 μl) of the same tryptic sample used in the previous SRM experiment was used to run the QTRAP 5500 mass spectrometer in the “precursor ion scanning mode” either for an ion at m/z 79 in negative ion mode for serine and threonine phosphorylation or an ion at m/z 216.043 for tyrosine phosphorylation in the positive ion mode. Once the precursor ions are detected, the instrument switches to positive ion trap scanning mode to isolate the parent ions and to perform MS2 analysis on these ions. The collected MS2 spectra were analyzed with the ProteinPilot search engine to identify the matching protein sequence from a database. The phosphorylation states of residues of the $G\alpha_{i3}$ protein were traced, and those that were used in this study are listed in Table 1.

Sequence alignment construction

For the sequence alignments (fig. S2), the amino acid sequences of human, mouse, and rat Gα proteins were downloaded from UniProt (97) using the query ‘family:”G-alpha family”‘ and were aligned with the modified version of the Needleman-Wunsch method (98) as implemented in the ICM software (99). The alignment was then projected to the amino acid positions of interest (residues 44, 47, 48, 151, 154, 155, and 320) of rat $G\alpha_{i3}$.

GiPCR-directed Gβγ activation assay

HeLa cells were cultured according to ATCC guidelines in DMEM supplemented with 10% FBS and an Antibiotic-Antimycotic solution. On day 1, the cells were plated at 800,000 cells per well in a 6-well plate in DMEM supplemented with 10% FBS. On day 2, the culture medium was replaced with fresh DMEM supplemented with 10% FBS, after which the cells were transfected with 0.5 μg/well VenusCT-Gβ, 0.5 μg/well VenusNT-Gγ, 1 μg/well of WT or mutant $G\alpha_{i3}$, and 100 ng/well of RLuc8-tagged GRK3ct (a total of approximately 2 μg/well of DNA) using the TransIT-X2 transfection reagent according to the manufacturer's instructions. On day 3, the cells were lifted from the wells with trypsin, transferred into 1.5-ml microcentrifuge tubes, spun down, and resuspended at 700,000 cells/ml in DMEM (no phenol red) supplemented with 10% FBS. Equal aliquots (100 μl/well, which is ~70,000 cells per well) of the cell suspension were replated in a 96-well white/clear bottom plate and allowed to adhere for 5 to 6 hours in a 37° 5% CO_2 incubator. For PTX-treated conditions, the culture medium was carefully removed from the wells and replaced with 100 μl/well of DMEM (no phenol red) supplemented with 10% FBS and 200 ng/mL PTX. On day 4, the culture medium was carefully removed from the wells and replaced with 80 μl/well of serum-free assay buffer (PBS with 0.1% D-Glucose and 0.05% BSA). The luciferase substrate Coelenterazine-h was added to each well (10 μl of a 0.1 mM stock to give a final concentration of 10 μM). The plate was incubated at room temperature for 5 min, after which repeated readings of light emission at 485 and 515 nm were initiated using the Spark 20M plate reader (Tecan Lifesciences) and continued for 3 min for basal reads. Next, the plate was taken out of the luminometer, 10 μl of either buffer or 1 μM CXCL12 (for a final concentration of 100 nM) were added to each well, and the plate was read for an additional 10 min to assess agonist-stimulated Gβγ activation. BRET at each time point was expressed as the intensity at 515 nm divided by the intensity at 485 nm. To generate basal Gβγ-GRK3ct association bar graphs, the results were integrated over the 3-min basal reads and normalized to the observed basal activity in the absence (pcDNA, set at 0%) or presence (PTX-sensitive WTs or and PTX-resistant WTr, set at 100%) exogenously expressed $G\alpha_{i3}$. For ligand-induced Gβγ-GRK3ct association, the reads were first baseline-corrected by subtracting the average of the basal reads and then integrated over 10 min after the addition of agonist (12 reads) and then normalized to the range of 0% (PTX-sensitive $G\alpha_{i3}$, WTs) to 100% (PTX-resistant $G\alpha_{i3}$, WTr). The experiment was repeated in four independent biological replicates on different days, each containing three technical replicates. To increase statistical power, in the basal association experiments, PTX-treated and untreated samples from the same day were used as separate biological replicates thus producing n = 8 samples. The findings were displayed as graphs with GraphPad Prism 9. An average of three to four biological replicates is shown in the figures.

CAMYEL $G\alpha_i$-directed cAMP suppression assay

On day 1, HeLa cells were plated at 600,000 cells per well in a 6-well plate in DMEM supplemented with 10% FBS. On day 2, the culture medium was replaced with fresh DMEM supplemented with 10% FBS, after which the cells were transfected with 0.5 μg/well WT or mutant Gαi, 1 μg/well of V2-CAMYEL (total: 1.5 μg/well of DNA) with the TransIT-X2 transfection reagent according to the manufacturer's instructions. On day 3, the cells were lifted from the wells with trypsin, transferred into 1.5-m microcentrifuge tubes,

and resuspended in DMEM with 10% FBS at a density of 700,000 cells/ml. Cell suspensions (100 μl/well; 70,000 cells per well) were replated onto a 96-well white/clear bottom plate and allowed to adhere for 5 to 6 hours in a 37°/5% CO_2 incubator. For PTX-treated conditions, the culture medium was carefully removed from the wells and replaced with 100 μl/well of DMEM (no phenol red) supplemented with 10%FBS and 200 ng/ml PTX. Cells were cultured in the incubator overnight. On day 4, the culture medium was carefully removed from the wells and replaced with 70 μl/well of serum-free assay buffer (PBS with 0.1% D-Glucose and 0.05% BSA). The luciferase substrate Coelenterazine-h was added to each well (10 μl of a 0.1 mM stock, to give a final concentration of 10 μM), together with 10 μL of a 1 mM stock of 3-isobutyl-1-methylxanthine (IBMX), to give a final concentration 100 μM IBMX. The plate was incubated at room temperature for 5 min, after which repeated readings of light emission at 485 and 515 nm were initiated with the SPARK 20M plate reader (Tecan) and continued for 3 min (to calculate the basal CAMYEL signal). Next, the plate was taken out of the luminometer and 10 μl of either buffer or 1 μM CXCL12 (to give a final concentration of 100 nM) were added to each well. The luminescence at 485 and 515 nm was immediately read for 6 min. Next, 10 μl of 100 μM forskolin (FSK; final in-well concentration: 10 μM) were added, and the 485/515 nm luminescence was read for another 15 min. The cAMP signal was calculated as the inverse BRET ratio (emission at 485 nm/emission at 515 nm). For the generation of bar graphs, the average 1/BRET over 3 to 6 min preceding FSK addition was subtracted from the average 1/BRET over the 10 to 12 min immediately after the addition of FSK. Results are expressed as the fold-change compared to the observed basal activity in the PTX-sensitive (WTs, set at 0%) and PTX-resistant (WTr, set at 100%) $G\alpha_{i3}$ in the PTX-treated condition. The experiment was repeated in four independent biological replicates on different days, each containing three technical replicates. The findings were displayed as graphs with GraphPad Prism 9. In the main figures, an average of three or four biological replicates is shown, whereas in fig. S4B, three separate biological replicates are shown.

Recruitment of mini-$G\alpha_{s/i}$ to CXCR4-Rluc3 (acceptor titration)

To study the recruitment of G protein to ligand-activated GPCR, we used an established BRET-based mini-$G\alpha_{s/i}$ recruitment assay (100). On day 1, HeLa cells were passaged and plated at 800,000 cells per well in 6-well tissue culture plates in DMEM supplemented with 10% FBS. On day 2, the cells were transfected with mixtures containing a fixed amount (100 ng/well) of HA-CXCR4-RLuc3 DNA (donor) and varying amounts (0, 156.25, 312.5, 625, 1250, and 2500 ng/well) of mVenus-mini$G\alpha_{s/i}$ WT, mVenus-mini$G\alpha_{s/i}$(Y320E) or mVenus-mini-$G\alpha_{s/i}$(Y320F) DNA (acceptor); the total amount of DNA was normalized to 2.6 μg/well with pcDNA. Transfections were performed with the TransIT-X2 transfection reagent according to the manufacturer's protocol. On day 3, the cells were lifted from the wells with trypsin, transferred into 1.5-ml microcentrifuge tubes, and resuspended in DMEM (without phenol red) supplemented with 10% FBS at a density of 800,000 cells/ml. Equal aliquots of cell suspension (100 μl/well; ~80,000 cells per well) were replated onto a 96-well white/clear bottom plate and allowed to adhere by keeping them in a37° incubator with 5% CO_2 supply. Additionally, for each transfected sample, 200,000 cells per well were plated into a 12-well plate for flow cytometric analysis. On the day of the assays, the medium was replaced with serum-free BRET assay buffer (PBS with 0.1% D-Glucose

and 0.05% BSA), coelenterazine-h was added to the wells to a final concentration of 10 μM, the plate was incubated for 2 min, and basal reads (emission at 485 nm and emission at 515 nm) were collected for 5 min in a SPARK 20M plate reader (Tecan). Next, either buffer or CXCL12 was added to the plate, the latter to a final concentration of 100 nM, and readings were recorded for an additional 10 min. The BRET ratio was calculated as the emission at 485 nm divided by emission at 515 nm. To generate bar graphs, BRET readings were baseline-corrected and control-subtracted (the former using reads preceding agonist addition, the latter, reads from buffer-treated wells), and the average over 5 to 8 readings (approximately 15 min) after CXCL12 addition was calculated. The experiment was repeated in five independent experiments on different days, each containing four technical replicates. The findings were displayed as graphs with GraphPad Prism 9. An average of five biological replicates is shown in the appropriate figures. For model fitting and parameter comparison between data-specific fit and global fit, we used an extra sum-of-squares F test as implemented in GraphPad Prism. For Lineweaver-Burk plot comparisons, we used the F-test to compute the significance of the non-zero slope, which was also implemented in GraphPad Prism.

Flow cytometry

Cells transfected for the mini-$G\alpha_{s/i}$ recruitment assay as described earlier were seeded at ~200,000 cells/well in a 12-well plate. On the next day, the cells were rinsed with PBS, detached with Accutase, and lifted in DMEM supplemented with 10% FBS, after which 300 μL of each cell suspension (containing ~100,000 cells) was transferred into a conical bottom, 96-well plate. The plate was centrifuged at 400*g* for 5 min, the supernatant aspirated, and the cells were resuspended in 200 μL/well of PBS with 0.5% BSA (flow buffer), which was performed twice. After the final spin, the cells were resuspended in 50 μl of flow buffer with the addition of a 1:50 dilution of APC-conjugated anti-HA antibody in PBS supplemented with 0.5% BSA; no antibody was added to the control well. Cells were stained on ice in the dark with rocking for 30 min and then washed twice with 200 μl/well of flow buffer. Finally, the cells were resuspended in 300 μl of flow buffer, and data were collected in a Guava EasyCyte benchtop flow cytometer (Luminex, USA). Data were analyzed with FlowJo software (10). A representative biological replicate of the flow cytometry analysis is shown in fig. S5, D to F.

Transwell cell migration assays

This assay is based on the Boyden Chamber method (101), which measures the chemotactic ability of cells through pores in a membrane insert toward a chemoattractant (in this case, CXCL12). On day 1, 1×10^6 HeLa cells per well were plated in a 6-well plate in DMEM supplemented with 10% FBS. On day 2, the cells were transfected with 2 μg/well DNA of WTs, WTr, and the other mutants. After 36 hours, the cells were treated with 100 ng/ml PTX for 12 hours. On the following day, the cells were rinsed in PBS, detached with trypsin, lifted in DMEM supplemented with 0.4% FBS, centrifuged, and resuspended in DMEM supplemented with 0.4% FBS. Cells were seeded in the top chamber of Transwell Polycarbonate (PC) translucent 8-μm pore inserts (Corning) in 24-well plates at a density of 300,000 cells per well in DMEM supplemented with 0.4% FBS. After 3 hours, CXCL12 was added to the bottom chamber at a final concentration of 40 nM. The cells were

incubated for an additional 20 hours in a 37°C incubator with a supply of 5% CO_2. This duration was chosen based on a previous study (55) as a reference, with further optimization in our own hands. On the following day, the supports were placed in a clean well containing 4% PFA for 1 hour at room temperature, stained with crystal violet for 1 hour, and washed three times in PBS. Cells on the upper side of the filters were removed with cotton-tipped swabs, and the number of cells that migrated on to the bottom side of the filter was counted in five randomly chosen fields at 200X magnification and averaged. All experiments were performed in triplicate, and each experiment was repeated at least three times.

Protein stability analysis

The mutation-induced changes in the stability of $G\alpha_i$ were calculated as differences in the free energy of folding between WT $G\alpha_i$ and its mutants. The calculations were performed with ICM (Molsoft LLC) using the _mutantStabilityAve tool and either GPCR-bound [PDB: 6cmo (72), 6ot0 (67)], GDP-bound [PDB: 1bof (102), 1gdd (103)), $G\beta\gamma$ bound [(PDB: 1gg2 (104)], or GTP bound [PDB: 1gia (105)] $G\alpha_i$ conformations. Predicted $\Delta\Delta G$ values were plotted as a bar graph, with higher/more positive values indicating a higher degree of predicted destabilizing effect of the mutation on the given conformation.

Confocal immunofluorescence microscopy

HeLa cells were plated on fibronectin-coated coverslips at 500,000 per well in a 6-well plate. On the next day, the cells were transfected with plasmids encoding the appropriate $G\alpha_{i3}$ mutants. Forty-eight hours later, the coverslips were washed with PBS, treated with 4% PFA for 30 min at room temperature, and washed a further three times with PBS. The coverslips were blocked in blocking buffer (PBS, 0.1% Triton-X-100, and 0.5% BSA) for 30 min and then incubated with a 1:100 dilution of the mouse monoclonal primary anti-$G\alpha_{i3}$ antibody (sc-365422, Santa Cruz) in blocking buffer overnight in a moist chamber at 4ºC. On the following day, the coverslips were rinsed three times in PBS, each time allowing for a 15-min incubation. The coverslips were then treated with Alexa Fluor 488–conjugated secondary antibody (at a 1:500 dilution) and DAPI (a stock of 1 mg/ml was diluted 1:2000 to give a final concentration of 500 ng/ml) in blocking buffer for 45 min at room temperature, which was followed by three rinses in PBS, each lasting 15 min. The coverslips were then blotted dry and mounted on a microscope slide with 5 μl of Prolong Glass Antifade reagent (Invitrogen). Transparent nail polish was applied to seal the coverslips on the microscope slide and hold them in position. Visualization was performed with an SPE confocal microscope (Leica) using a 63X oil objective using 488- and 405-nm lasers for excitation. Approximately 10 images were collected for each construct. The settings were optimized, and the final images were scanned with a line-averaging of three. All images were processed with ImageJ software (NIH) and assembled for presentation with Photoshop and Illustrator software (Adobe).

Cytosolic and membrane fractionation

HeLa cells were plated in 10-cm dishes at 2×10^6 cells per dish in DMEM supplemented with 10% FBS. On the next day, the cells were transfected with 8 μg/dish of total plasmid DNA for $G\alpha_{i3}$(C351I) or the appropriate phosphomutants with polyethylenimine (PEI), as described previously (106). After 48 hours, the cells were rinsed once with PBS and

lifted using a cell scraper in homogenization buffer [25 mM HEPES-KOH, 250 mM sucrose, 1 mM EDTA, (pH 7.4)] supplemented with protease and phosphatase inhibitors. Approximately 150 μl of homogenization buffer was used per 10-cm dish of cells. A 30–1/2 G syringe was used to break the cells by passing them through the needle ~40 times (10 times/set with a 5-min rest time in-between each set, for a total of 4 sets). The cell suspension was then spun down at 500g for 10 min (to remove the nuclear pellet), after which the supernatant was collected and transferred into a 1.7-ml, thick-walled ultracentrifuge tube and ultracentrifuged at 100,000*g* for 60 min. The resultant supernatant was collected as the cytosolic fraction. The resultant pellet (crude membrane fraction) was rinsed further with homogenization buffer and centrifuged at 100,000*g* for 30 min, and the pellet was subsequently resuspended in lysis buffer [20 mM HEPES, (pH 7.2), 5 mM magnesium acetate, 125 mM potassium acetate, 0.4% Triton X-100, 1 mM DTT, supplemented with sodium orthovanadate (500 μM), phosphatase (Sigma), and protease (Roche) inhibitor cocktails]. The proteins were quantified, and 10% of each fraction was loaded onto a 12% SDS PAGE gel and analyzed by Western blotting with anti-$G\alpha_{i3}$ antibody (11641–1-AP, ProteinTech) and pan anti-$G\beta\gamma$ antibody (sc 378, Santa Cruz).

Quantitative Western blotting

For Western blotting, proteins were resolved by SDS-PAGE and transferred onto 0.4-μm PVDF membranes (Millipore, MA). Membranes were blocked with PBS, 5% nonfat milk (blocking buffer) before incubation with primary antibodies. Primary antibodies were prepared in blocking buffer containing 0.1% Tween-20 and incubated with the blots overnight at 4ºC with rocking. After incubation, the blots were washed and incubated with secondary antibodies for 1 hour at room temperature, washed again, and imaged with a dual-color Li-Cor Odyssey imaging system (Li-Cor, USA). All Odyssey images were processed with Image J software (NIH) and assembled for presentation using Photoshop and Illustrator software (Adobe).

Image-processing

All images were processed with ImageJ software (NIH) or FlowJo software and assembled into figure panels with Photoshop and Illustrator (Adobe Creative Cloud). All graphs were generated with GraphPad Prism v9.

Statistical analysis

All experiments were performed at least three times, and results are presented either as average ± SEM or with boundaries for 95% confidence interval (CI). Statistical significance was assessed with F-tests for model fitting and regression analysis and by one-way analysis of variance (ANOVA) including a Tukey's test for multiple comparisons. In general, exact *P* values are shown throughout the work. Otherwise, statistical significance is denoted as follows: $*P < 0.05$, $**P < 0.01$, $***P < 0.001$, $****P < 0.0001$.

Supplementary Material

Refer to Web version on PubMed Central for supplementary material.

Acknowledgments:

We thank A. Spiegel (National Institutes of Health, Bethesda, MD), P. Insel and T. M. Handel (UC San Diego, CA, USA), N. A. Lambert (Augusta University, GA, USA), M. Bouvier (Université de Montréal, Canada), and S. Lanier (University of South Carolina) for their generosity in sharing receptor and reporter constructs, and T. M. Handel (UC San Diego, CA, USA) for sharing access to the Guava benchtop flow cytometer.

Funding:

This paper was supported by the NIH (CA238042, AI141630, CA100768, and CA160911 to P.G.; R21 AI149369, R01 GM136202, R21 AI156662, and R01 AI161880 to I.K.). S.S was supported through The American Association of Immunologists (AAI) Intersect Fellowship Program for Computational Scientist and Immunobiologists.

Data and materials availability:

All data needed to evaluate the conclusions in the paper are present in the paper or the Supplementary Materials.

References and Notes

1. Vert G, Chory J, Crosstalk in cellular signaling: background noise or the real thing? Developmental cell 21, 985–991 (2011); published online EpubDec 13 (10.1016/j.devcel.2011.11.006). [PubMed: 22172668]
2. Logue JS, Morrison DK, Complexity in the signaling network: insights from the use of targeted inhibitors in cancer therapy. Genes & development 26, 641–650 (2012); published online EpubApr 1 (10.1101/gad.186965.112). [PubMed: 22474259]
3. Siso-Nadal F, Fox JJ, Laporte SA, Hébert TE, Swain PS, Cross-talk between signaling pathways can generate robust oscillations in calcium and cAMP. PloS one 4, e7189 (2009); published online EpubOct 21 (10.1371/journal.pone.0007189).
4. Tsunoda S, Sierralta J, Zuker CS, Specificity in signaling pathways: assembly into multimolecular signaling complexes. Current opinion in genetics & development 8, 419–422 (1998); published online EpubAug (10.1016/s0959-437x(98)80112-3). [PubMed: 9729717]
5. Kalogriopoulos NA, Lopez-Sanchez I, Lin C, Ngo T, Midde KK, Roy S, Aznar N, Murray F, Garcia-Marcos M, Kufareva I, Ghassemian M, Ghosh P, Receptor tyrosine kinases activate heterotrimeric G proteins via phosphorylation within the interdomain cleft of Gαi. Proc Natl Acad Sci U S A 117, 28763–28774 (2020); published online EpubNov 17 (10.1073/pnas.2004699117). [PubMed: 33139573]
6. Bennasroune A, Gardin A, Aunis D, Crémel G, Hubert P, Tyrosine kinase receptors as attractive targets of cancer therapy. Critical Reviews in Oncology/Hematology 50, 23–38 (2004); published online Epub2004/04/01/ (10.1016/j.critrevonc.2003.08.004). [PubMed: 15094157]
7. Gilman AG, G proteins: transducers of receptor-generated signals. Annual review of biochemistry 56, 615–649 (1987)10.1146/annurev.bi.56.070187.003151).
8. Morris AJ, Malbon CC, Physiological regulation of G protein-linked signaling. Physiological reviews 79, 1373–1430 (1999); published online EpubOct (10.1152/physrev.1999.79.4.1373). [PubMed: 10508237]
9. Lowes VL, Ip NY, Wong YH, Integration of signals from receptor tyrosine kinases and g protein-coupled receptors. Neuro-Signals 11, 5–19 (2002); published online EpubJan-Feb (10.1159/000057317). [PubMed: 11943878]
10. Piiper A, Zeuzem S, Receptor tyrosine kinases are signaling intermediates of G protein-coupled receptors. Curr Pharm Des 10, 3539–3545 (2004); published online Epub2004 (10.2174/1381612043382936). [PubMed: 15579051]
11. Natarajan K, Berk BC, Crosstalk coregulation mechanisms of G protein-coupled receptors and receptor tyrosine kinases. Methods in molecular biology (Clifton, N.J.) 332, 51–77 (2006)10.1385/1-59745-048-0:51).

12. Shah BH, Catt KJ, GPCR-mediated transactivation of RTKs in the CNS: mechanisms and consequences. Trends in neurosciences 27, 48–53 (2004); published online EpubJan (10.1016/j.tins.2003.11.003). [PubMed: 14698610]
13. Di Liberto V, Mudò G, Belluardo N, Crosstalk between receptor tyrosine kinases (RTKs) and G protein-coupled receptors (GPCR) in the brain: Focus on heteroreceptor complexes and related functional neurotrophic effects. Neuropharmacology 152, 67–77 (2019); published online EpubJul 1 (10.1016/j.neuropharm.2018.11.018). [PubMed: 30445101]
14. Daub H, Weiss FU, Wallasch C, Ullrich A, Role of transactivation of the EGF receptor in signalling by G-protein-coupled receptors. Nature 379, 557–560 (1996); published online EpubFeb 8 (10.1038/379557a0). [PubMed: 8596637]
15. Luttrell LM, Daaka Y, Lefkowitz RJ, Regulation of tyrosine kinase cascades by G-protein-coupled receptors. Curr Opin Cell Biol 11, 177–183 (1999); published online EpubApr (10.1016/s0955-0674(99)80023-4). [PubMed: 10209148]
16. Schäfer B, Gschwind A, Ullrich A, Multiple G-protein-coupled receptor signals converge on the epidermal growth factor receptor to promote migration and invasion. Oncogene 23, 991–999 (2004); published online EpubJan 29 (10.1038/sj.onc.1207278). [PubMed: 14647423]
17. Ohtsu H, Dempsey PJ, Eguchi S, ADAMs as mediators of EGF receptor transactivation by G protein-coupled receptors. American journal of physiology. Cell physiology 291, C1–10 (2006); published online EpubJul (10.1152/ajpcell.00620.2005). [PubMed: 16769815]
18. Prenzel N, Zwick E, Daub H, Leserer M, Abraham R, Wallasch C, Ullrich A, EGF receptor transactivation by G-protein-coupled receptors requires metalloproteinase cleavage of proHB-EGF. Nature 402, 884–888 (1999); published online EpubDec 23–30 (10.1038/47260). [PubMed: 10622253]
19. Guidolin D, Agnati LF, Marcoli M, Borroto-Escuela DO, Fuxe K, G-protein-coupled receptor type A heteromers as an emerging therapeutic target. Expert opinion on therapeutic targets 19, 265–283 (2015); published online EpubFeb (10.1517/14728222.2014.981155). [PubMed: 25381716]
20. Sun H, Seyer JM, Patel TB, A region in the cytosolic domain of the epidermal growth factor receptor antithetically regulates the stimulatory and inhibitory guanine nucleotide-binding regulatory proteins of adenylyl cyclase. 92, 2229–2233 (1995)doi:10.1073/pnas.92.6.2229).
21. Poppleton H, Sun H, Fulgham D, Bertics P, Patel TB, Activation of Gsalpha by the epidermal growth factor receptor involves phosphorylation. J Biol Chem 271, 6947–6951 (1996); published online EpubMar 22 (10.1074/jbc.271.12.6947). [PubMed: 8636123]
22. Marty C, Ye RD, Heterotrimeric G protein signaling outside the realm of seven transmembrane domain receptors. Molecular pharmacology 78, 12–18 (2010); published online EpubJul (10.1124/mol.110.063453). [PubMed: 20404072]
23. Nair BG, Parikh B, Milligan G, Patel TB, Gs alpha mediates epidermal growth factor-elicited stimulation of rat cardiac adenylate cyclase. J Biol Chem 265, 21317–21322 (1990); published online EpubDec 5 ([PubMed: 2123491]
24. Sun H, Chen Z, Poppleton H, Scholich K, Mullenix J, Weipz GJ, Fulgham DL, Bertics PJ, Patel TB, The juxtamembrane, cytosolic region of the epidermal growth factor receptor is involved in association with alpha-subunit of Gs. J Biol Chem 272, 5413–5420 (1997); published online EpubFeb 28 ([PubMed: 9038141]
25. Zick Y, Sagi-Eisenberg R, Pines M, Gierschik P, Spiegel AM, Multisite phosphorylation of the alpha subunit of transducin by the insulin receptor kinase and protein kinase C. Proc Natl Acad Sci U S A 83, 9294–9297 (1986); published online EpubDec (10.1073/pnas.83.24.9294). [PubMed: 3099281]
26. Krupinski J, Rajaram R, Lakonishok M, Benovic JL, Cerione RA, Insulin-dependent phosphorylation of GTP-binding proteins in phospholipid vesicles. Journal of Biological Chemistry 263, 12333–12341 (1988)10.1016/S0021-9258(18)37759-7). [PubMed: 3137226]
27. Hausdorff WP, Pitcher JA, Luttrell DK, Linder ME, Kurose H, Parsons SJ, Caron MG, Lefkowitz RJ, Tyrosine phosphorylation of G protein alpha subunits by pp60c-src. Proc Natl Acad Sci U S A 89, 5720–5724 (1992); published online EpubJul 1 (10.1073/pnas.89.13.5720). [PubMed: 1378615]

28. Umemori H, Inoue T, Kume S, Sekiyama N, Nagao M, Itoh H, Nakanishi S, Mikoshiba K, Yamamoto T, Activation of the G protein Gq/11 through tyrosine phosphorylation of the alpha subunit. Science 276, 1878–1881 (1997); published online EpubJun 20 (10.1126/science.276.5320.1878). [PubMed: 9188537]
29. Ghosh P, Mullick M, Building unconventional G protein-coupled receptors, one block at a time. Trends Pharmacol Sci 42, 514–517 (2021); published online EpubJul (10.1016/j.tips.2021.04.005). [PubMed: 33985816]
30. Midde KK, Aznar N, Laederich MB, Ma GS, Kunkel MT, Newton AC, Ghosh P, Multimodular biosensors reveal a novel platform for activation of G proteins by growth factor receptors. Proc Natl Acad Sci U S A 112, E937–946 (2015); published online EpubMar 3 (10.1073/pnas.1420140112). [PubMed: 25713130]
31. Lin C, Ear J, Midde K, Lopez-Sanchez I, Aznar N, Garcia-Marcos M, Kufareva I, Abagyan R, Ghosh P, Structural basis for activation of trimeric Gi proteins by multiple growth factor receptors via GIV/Girdin. Molecular biology of the cell 25, 3654–3671 (2014); published online Epub2014/11// (10.1091/mbc.e14-05-0978). [PubMed: 25187647]
32. Neves M, Perpiñá-Viciano C, Penela P, Hoffmann C, Mayor F Jr., Modulation of CXCR4-Mediated Gi1 Activation by EGF Receptor and GRK2. ACS Pharmacol Transl Sci 3, 627–634 (2020); published online EpubAug 14 (10.1021/acsptsci.0c00021). [PubMed: 33073183]
33. Kim HG, Jeong SG, Kim JH, Cho JY, Phosphatase inhibition by sodium orthovanadate displays anti-inflammatory action by suppressing AKT-IKKβ signaling in RAW264.7 cells. Toxicology reports 9, 1883–1893 (2022)10.1016/j.toxrep.2022.09.012). [PubMed: 36518371]
34. Douglas DJ, Frank AJ, Mao D, Linear ion traps in mass spectrometry. Mass spectrometry reviews 24, 1–29 (2005); published online EpubJan-Feb (10.1002/mas.20004). [PubMed: 15389865]
35. Berman DM, Wilkie TM, Gilman AG, GAIP and RGS4 are GTPase-activating proteins for the Gi subfamily of G protein alpha subunits. Cell 86, 445–452 (1996); published online EpubAug 9 (10.1016/s0092-8674(00)80117-8). [PubMed: 8756726]
36. Kobilka BK, Kobilka TS, Daniel K, Regan JW, Caron MG, Lefkowitz RJ, Chimeric alpha 2-,beta 2-adrenergic receptors: delineation of domains involved in effector coupling and ligand binding specificity. Science 240, 1310–1316 (1988); published online EpubJun 3 (10.1126/science.2836950). [PubMed: 2836950]
37. De Vries L, Fischer T, Tronchère H, Brothers GM, Strockbine B, Siderovski DP, Farquhar MG, Activator of G protein signaling 3 is a guanine dissociation inhibitor for Gαi subunits. Proceedings of the National Academy of Sciences 97, 14364–14369 (2000); published online Epub2000/12/19 (10.1073/pnas.97.26.14364).
38. Oner SS, Maher EM, Gabay M, Tall GG, Blumer JB, Lanier SM, Regulation of the G-protein regulatory-Gαi signaling complex by nonreceptor guanine nucleotide exchange factors. J Biol Chem 288, 3003–3015 (2013); published online EpubFeb 1 (10.1074/jbc.M112.418467). [PubMed: 23212907]
39. Garcia-Marcos M, Ghosh P, Farquhar MG, GIV is a nonreceptor GEF for Gαi with a unique motif that regulates Akt signaling. Proceedings of the National Academy of Sciences 106, 3178–3183 (2009); published online Epub2009/03/03 (10.1073/pnas.0900294106).
40. Gupta V, Bhandari D, Leyme A, Aznar N, Midde KK, Lo IC, Ear J, Niesman I, López-Sánchez I, Blanco-Canosa JB, von Zastrow M, Garcia-Marcos M, Farquhar MG, Ghosh P, GIV/Girdin activates Gαi and inhibits Gαs via the same motif. Proceedings of the National Academy of Sciences 113, E5721–E5730 (2016); published online Epub2016/09/27 (10.1073/pnas.1609502113).
41. Bhola NE, Grandis JR, Crosstalk between G-protein-coupled receptors and epidermal growth factor receptor in cancer. Frontiers in bioscience : a journal and virtual library 13, 1857–1865 (2008); published online EpubJan 1 (10.2741/2805). [PubMed: 17981673]
42. Kilpatrick LE, Hill SJ, Transactivation of G protein-coupled receptors (GPCRs) and receptor tyrosine kinases (RTKs): Recent insights using luminescence and fluorescence technologies. Current Opinion in Endocrine and Metabolic Research 16, 102–112 (2021); published online Epub2021/02/01/ (10.1016/j.coemr.2020.10.003). [PubMed: 33748531]
43. Oda K, Matsuoka Y, Funahashi A, Kitano H, A comprehensive pathway map of epidermal growth factor receptor signaling. 1, 2005.0010 (2005)10.1038/msb4100014).

44. Sun D, Flock T, Deupi X, Maeda S, Matkovic M, Mendieta S, Mayer D, Dawson R, Schertler GFX, Madan Babu M, Veprintsev DB, Probing Gαi1 protein activation at single-amino acid resolution. Nat Struct Mol Biol 22, 686–694 (2015); published online EpubSep (10.1038/nsmb.3070). [PubMed: 26258638]
45. Liang MN, Garrison JC, The epidermal growth factor receptor is coupled to a pertussis toxin-sensitive guanine nucleotide regulatory protein in rat hepatocytes. Journal of Biological Chemistry 266, 13342–13349 (1991); published online Epub1991/07/15/ (10.1016/S0021-9258(18)98845-9). [PubMed: 1649188]
46. O'Brien RM, Houslay MD, Milligan G, Siddle K, The insulin receptor tyrosyl kinase phosphorylates holomeric forms of the guanine nucleotide regulatory proteins Gi and Go. FEBS letters 212, 281–288 (1987); published online EpubFeb 23 (10.1016/0014-5793(87)81361-3). [PubMed: 3028864]
47. Chen Z, Cole PA, Synthetic approaches to protein phosphorylation. Current opinion in chemical biology 28, 115–122 (2015); published online EpubOct (10.1016/j.cbpa.2015.07.001). [PubMed: 26196731]
48. Carty DJ, Pertussis toxin-catalyzed ADP-ribosylation of G proteins. Methods Enzymol 237, 63–70 (1994)10.1016/s0076-6879(94)37053-2). [PubMed: 7935025]
49. Mangmool S, Kurose H, G(i/o) protein-dependent and -independent actions of Pertussis Toxin (PTX). Toxins 3, 884–899 (2011); published online EpubJul (10.3390/toxins3070884). [PubMed: 22069745]
50. Neptune ER, Iiri T, Bourne HR, Galphai is not required for chemotaxis mediated by Gi-coupled receptors. J Biol Chem 274, 2824–2828 (1999); published online EpubJan 29 (10.1074/jbc.274.5.2824). [PubMed: 9915816]
51. Busillo JM, Benovic JL, Regulation of CXCR4 signaling. Biochimica et biophysica acta 1768, 952–963 (2007); published online EpubApr (10.1016/j.bbamem.2006.11.002). [PubMed: 17169327]
52. Cheng Y, Che X, Zhang S, Guo T, He X, Liu Y, Qu X, Positive Cross-Talk Between CXC Chemokine Receptor 4 (CXCR4) and Epidermal Growth Factor Receptor (EGFR) Promotes Gastric Cancer Metastasis via the Nuclear Factor kappa B (NF-kB)-Dependent Pathway. Medical science monitor : international medical journal of experimental and clinical research 26, e925019 (2020); published online EpubSep 3 (10.12659/msm.925019).
53. Smit MJ, Schlecht-Louf G, Neves M, van den Bor J, Penela P, Siderius M, Bachelerie F, Mayor F Jr., The CXCL12/CXCR4/ACKR3 Axis in the Tumor Microenvironment: Signaling, Crosstalk, and Therapeutic Targeting. Annual review of pharmacology and toxicology 61, 541–563 (2021); published online EpubJan 6 (10.1146/annurev-pharmtox-010919-023340).
54. Wang C, Cheng H, Li Y, Role of SDF-1 and CXCR4 in the proliferation, migration and invasion of cervical cancer. Pakistan journal of pharmaceutical sciences 29, 2151–2154 (2016); published online EpubNov ([PubMed: 28412671]
55. Dillenburg-Pilla P, Patel V, Mikelis CM, Zarate-Blades CR, Doci CL, Amornphimoltham P, Wang Z, Martin D, Leelahavanichkul K, Dorsam RT, Masedunskas A, Weigert R, Molinolo AA, Gutkind JS, SDF-1/CXCL12 induces directional cell migration and spontaneous metastasis via a CXCR4/Galphai/mTORC1 axis. FASEB J 29, 1056–1068 (2015); published online EpubMar (10.1096/fj.14-260083). [PubMed: 25466898]
56. Nguyen HT, Reyes-Alcaraz A, Yong HJ, Nguyen LP, Park HK, Inoue A, Lee CS, Seong JY, Hwang JI, CXCR7: a β-arrestin-biased receptor that potentiates cell migration and recruits β-arrestin2 exclusively through Gβγ subunits and GRK2. Cell & bioscience 10, 134 (2020); published online EpubNov 23 (10.1186/s13578-020-00497-x). [PubMed: 33292475]
57. White CW, Caspar B, Vanyai HK, Pfleger KDG, Hill SJ, CRISPR-Mediated Protein Tagging with Nanoluciferase to Investigate Native Chemokine Receptor Function and Conformational Changes. Cell chemical biology 27, 499–510.e497 (2020); published online EpubMay 21 (10.1016/j.chembiol.2020.01.010). [PubMed: 32053779]
58. Xu L, Li C, Hua F, Liu X, The CXCL12/CXCR7 signalling axis promotes proliferation and metastasis in cervical cancer. Medical Oncology 38, 58 (2021); published online Epub2021/04/13 (10.1007/s12032-021-01481-2). [PubMed: 33847822]

59. Canals M, Scholten DJ, de Munnik S, Han MK, Smit MJ, Leurs R, Ubiquitination of CXCR7 controls receptor trafficking. PloS one 7, e34192 (2012)10.1371/journal.pone.0034192).
60. Meyrath M, Szpakowska M, Zeiner J, Massotte L, Merz MP, Benkel T, Simon K, Ohnmacht J, Turner JD, Krüger R, Seutin V, Ollert M, Kostenis E, Chevigné A, The atypical chemokine receptor ACKR3/CXCR7 is a broad-spectrum scavenger for opioid peptides. Nat Commun 11, 3033 (2020); published online EpubJun 19 (10.1038/s41467-020-16664-0). [PubMed: 32561830]
61. Rajagopal S, Kim J, Ahn S, Craig S, Lam CM, Gerard NP, Gerard C, Lefkowitz RJ, β-arrestin- but not G protein-mediated signaling by the "decoy" receptor CXCR7. 107, 628–632 (2010)doi:10.1073/pnas.0912852107). [PubMed: 20018651]
62. Martemyanov KA, Mechanisms of Gβγ Release upon GPCR Activation. Trends Biochem Sci 46, 703–704 (2021); published online EpubSep (10.1016/j.tibs.2021.05.002). [PubMed: 34034924]
63. Bachelerie F, Ben-Baruch A, Burkhardt AM, Combadiere C, Farber JM, Graham GJ, Horuk R, Sparre-Ulrich AH, Locati M, Luster AD, Mantovani A, Matsushima K, Murphy PM, Nibbs R, Nomiyama H, Power CA, Proudfoot AE, Rosenkilde MM, Rot A, Sozzani S, Thelen M, Yoshie O, Zlotnik A, International Union of Basic and Clinical Pharmacology. [corrected]. LXXXIX. Update on the extended family of chemokine receptors and introducing a new nomenclature for atypical chemokine receptors. Pharmacological reviews 66, 1–79 (2014)10.1124/pr.113.007724). [PubMed: 24218476]
64. Lambert NA, Johnston CA, Cappell SD, Kuravi S, Kimple AJ, Willard FS, Siderovski DP, Regulators of G-protein Signaling accelerate GPCR signaling kinetics and govern sensitivity solely by accelerating GTPase activity. 107, 7066–7071 (2010)doi:10.1073/pnas.0912934107).
65. Masuho I, Martemyanov KA, Lambert NA, in G Protein-Coupled Receptors in Drug Discovery: Methods and Protocols, Filizola M, Ed. (Springer New York, New York, NY, 2015), pp. 107–113.
66. Masuho I, Ostrovskaya O, Kramer GM, Jones CD, Xie K, Martemyanov KA, Distinct profiles of functional discrimination among G proteins determine the actions of G protein–coupled receptors. 8, ra123–ra123 (2015)doi:10.1126/scisignal.aab4068).
67. Qi X, Liu H, Thompson B, McDonald J, Zhang C, Li X, Cryo-EM structure of oxysterol-bound human Smoothened coupled to a heterotrimeric Gi. Nature 571, 279–283 (2019); published online Epub2019/07/01 (10.1038/s41586-019-1286-0). [PubMed: 31168089]
68. Draper-Joyce CJ, Khoshouei M, Thal DM, Liang Y-L, Nguyen ATN, Furness SGB, Venugopal H, Baltos J-A, Plitzko JM, Danev R, Baumeister W, May LT, Wootten D, Sexton PM, Glukhova A, Christopoulos A, Structure of the adenosine-bound human adenosine A1 receptor–Gi complex. Nature 558, 559–563 (2018); published online Epub2018/06/01 (10.1038/s41586-018-0236-6). [PubMed: 29925945]
69. Liang YL, Zhao P, Draper-Joyce C, Baltos JA, Glukhova A, Truong TT, May LT, Christopoulos A, Wootten D, Sexton PM, Furness SGB, Dominant Negative G Proteins Enhance Formation and Purification of Agonist-GPCR-G Protein Complexes for Structure Determination. ACS Pharmacol Transl Sci 1, 12–20 (2018); published online EpubSep 14 (10.1021/acsptsci.8b00017). [PubMed: 32219201]
70. Murphy PM, Baggiolini M, Charo IF, Hébert CA, Horuk R, Matsushima K, Miller LH, Oppenheim JJ, Power CA, International union of pharmacology. XXII. Nomenclature for chemokine receptors. Pharmacological reviews 52, 145–176 (2000); published online EpubMar ([PubMed: 10699158]
71. Jiang LI, Collins J, Davis R, Lin KM, DeCamp D, Roach T, Hsueh R, Rebres RA, Ross EM, Taussig R, Fraser I, Sternweis PC, Use of a cAMP BRET sensor to characterize a novel regulation of cAMP by the sphingosine 1-phosphate/G13 pathway. J Biol Chem 282, 10576–10584 (2007); published online EpubApr 6 (10.1074/jbc.M609695200). [PubMed: 17283075]
72. Kang Y, Kuybeda O, de Waal PW, Mukherjee S, Van Eps N, Dutka P, Zhou XE, Bartesaghi A, Erramilli S, Morizumi T, Gu X, Yin Y, Liu P, Jiang Y, Meng X, Zhao G, Melcher K, Ernst OP, Kossiakoff AA, Subramaniam S, Xu HE, Cryo-EM structure of human rhodopsin bound to an inhibitory G protein. Nature 558, 553–558 (2018); published online EpubJun (10.1038/s41586-018-0215-y). [PubMed: 29899450]
73. Wan Q, Okashah N, Inoue A, Nehmé R, Carpenter B, Tate CG, Lambert NA, Mini G protein probes for active G protein-coupled receptors (GPCRs) in live cells. J Biol Chem 293, 7466–7473 (2018); published online EpubMay 11 (10.1074/jbc.RA118.001975). [PubMed: 29523687]

74. Akekawatchai C, Holland JD, Kochetkova M, Wallace JC, McColl SR, Transactivation of CXCR4 by the insulin-like growth factor-1 receptor (IGF-1R) in human MDA-MB-231 breast cancer epithelial cells. J Biol Chem 280, 39701–39708 (2005); published online EpubDec 2 (10.1074/jbc.M509829200). [PubMed: 16172123]
75. Wright SJ, Inchausti R, Eaton CJ, Krystofova S, Borkovich KA, RIC8 is a guanine-nucleotide exchange factor for Galpha subunits that regulates growth and development in Neurospora crassa. Genetics 189, 165–176 (2011); published online EpubSep (10.1534/genetics.111.129270). [PubMed: 21750256]
76. McClelland LJ, Zhang K, Mou T-C, Johnston J, Yates-Hansen C, Li S, Thomas CJ, Doukov TI, Triest S, Wohlkonig A, Tall GG, Steyaert J, Chiu W, Sprang SR, Structure of the G protein chaperone and guanine nucleotide exchange factor Ric-8A bound to Gαi1. Nature Communications 11, 1077 (2020); published online Epub2020/02/26 (10.1038/s41467-020-14943-4).
77. Lo IC, Gupta V, Midde KK, Taupin V, Lopez-Sanchez I, Kufareva I, Abagyan R, Randazzo PA, Farquhar MG, Ghosh P, Activation of Gαi at the Golgi by GIV/Girdin imposes finiteness in Arf1 signaling. Developmental cell 33, 189–203 (2015); published online EpubApr 20 (10.1016/j.devcel.2015.02.009). [PubMed: 25865347]
78. Dror RO, Mildorf TJ, Hilger D, Manglik A, Borhani DW, Arlow DH, Philippsen A, Villanueva N, Yang Z, Lerch MT, Hubbell WL, Kobilka BK, Sunahara RK, Shaw DE, SIGNAL TRANSDUCTION. Structural basis for nucleotide exchange in heterotrimeric G proteins. Science 348, 1361–1365 (2015); published online EpubJun 19 (10.1126/science.aaa5264). [PubMed: 26089515]
79. Sprang SR, Invited review: Activation of G proteins by GTP and the mechanism of Galpha-catalyzed GTP hydrolysis. Biopolymers 105, 449–462 (2016); published online EpubAug (10.1002/bip.22836). [PubMed: 26996924]
80. Saraste M, Sibbald PR, Wittinghofer A, The P-loop — a common motif in ATP- and GTP-binding proteins. Trends in Biochemical Sciences 15, 430–434 (1990); published online Epub1990/11/01/(10.1016/0968-0004(90)90281-F). [PubMed: 2126155]
81. Chu J, Zheng H, Zhang Y, Loh HH, Law PY, Agonist-dependent mu-opioid receptor signaling can lead to heterologous desensitization. Cell Signal 22, 684–696 (2010); published online EpubApr (10.1016/j.cellsig.2009.12.003). [PubMed: 20043990]
82. Marivin A, Leyme A, Parag-Sharma K, DiGiacomo V, Cheung AY, Nguyen LT, Dominguez I, Garcia-Marcos M, Dominant-negative Galpha subunits are a mechanism of dysregulated heterotrimeric G protein signaling in human disease. Science signaling 9, ra37 (2016); published online EpubApr 12 (10.1126/scisignal.aad2429).
83. Navarro L, Koller A, Nordfelth R, Wolf-Watz H, Taylor S, Dixon JE, Identification of a molecular target for the Yersinia protein kinase A. Mol Cell 26, 465–477 (2007); published online EpubMay 25 (10.1016/j.molcel.2007.04.025). [PubMed: 17531806]
84. Afshar K, Willard FS, Colombo K, Siderovski DP, P. Gönczy, Cortical localization of the Gα protein GPA-16 requires RIC-8 function during C. elegans asymmetric cell division. Development 132, 4449–4459 (2005)10.1242/dev.02039%JDevelopment). [PubMed: 16162648]
85. David NB, Martin CA, Segalen M, Rosenfeld F, Schweisguth F, Bellaïche Y, Drosophila Ric-8 regulates Gαi cortical localization to promote Gαi-dependent planar orientation of the mitotic spindle during asymmetric cell division. Nature Cell Biology 7, 1083–1090 (2005); published online Epub2005/11/01 (10.1038/ncb1319). [PubMed: 16228010]
86. Gabay M, Pinter ME, Wright FA, Chan P, Murphy AJ, Valenzuela DM, Yancopoulos GD, Tall GG, Ric-8 Proteins Are Molecular Chaperones That Direct Nascent G Protein α Subunit Membrane Association. 4, ra79–ra79 (2011)doi:10.1126/scisignal.2002223).
87. Hampoelz B, Hoeller O, Bowman SK, Dunican D, Knoblich JA, Drosophila Ric-8 is essential for plasma-membrane localization of heterotrimeric G proteins. Nature Cell Biology 7, 1099–1105 (2005); published online Epub2005/11/01 (10.1038/ncb1318). [PubMed: 16228011]
88. Wang H, Ng KH, Qian H, Siderovski DP, Chia W, Yu F, Ric-8 controls Drosophila neural progenitor asymmetric division by regulating heterotrimeric G proteins. Nat Cell Biol 7, 1091–1098 (2005); published online EpubNov (10.1038/ncb1317). [PubMed: 16228012]

89. Ghosh P, Garcia-Marcos M, Bornheimer SJ, Farquhar Activation of MG $G\alpha_{i3}$ triggers cell migration via regulation of GIV. Journal of Cell Biology 182, 381–393 (2008)10.1083/jcb.200712066%JJournalofCellBiology). [PubMed: 18663145]

90. Bondar A, Lazar J, Dissociated GalphaGTP and Gbetagamma protein subunits are the major activated form of heterotrimeric Gi/o proteins. J Biol Chem 289, 1271–1281 (2014); published online EpubJan 17 (10.1074/jbc.M113.493643). [PubMed: 24307173]

91. Hunter MR, Finlay DB, Macdonald CE, Cawston EE, Grimsey NL, Glass M, Real-Time Measurement of Cannabinoid Receptor-Mediated cAMP Signaling. Methods Enzymol 593, 43–59 (2017)10.1016/bs.mie.2017.05.001). [PubMed: 28750814]

92. Ngo T, Stephens BS, Gustavsson M, Holden LG, Abagyan R, Handel TM, Kufareva I, Crosslinking-guided geometry of a complete CXC receptor-chemokine complex and the basis of chemokine subfamily selectivity. PLOS Biology 18, e3000656 (2020)10.1371/journal.pbio.3000656).

93. Brown NE, Lambert NA, Hepler JR, RGS14 regulates the lifetime of Gα-GTP signaling but does not prolong Gβγ signaling following receptor activation in live cells. Pharmacol Res Perspect 4, e00249-e00249 (2016)10.1002/prp2.249).

94. Ghosh P, Garcia-Marcos M, Bornheimer SJ, Farquhar MG, Activation of $Galpha_{i3}$ triggers cell migration via regulation of GIV. J Cell Biol 182, 381–393 (2008); published online EpubJul 28 (10.1083/jcb.200712066). [PubMed: 18663145]

95. Garcia-Marcos M, Ghosh P, Ear J, Farquhar MG, A structural determinant that renders G alpha(i) sensitive to activation by GIV/girdin is required to promote cell migration. J Biol Chem 285, 12765–12777 (2010); published online EpubApr 23 (10.1074/jbc.M109.045161). [PubMed: 20157114]

96. Garcia-Marcos M, Ear J, Farquhar MG, Ghosh P, A GDI (AGS3) and a GEF (GIV) regulate autophagy by balancing G protein activity and growth factor signals. Mol Biol Cell 22, 673–686 (2011); published online EpubMar 1 (10.1091/mbc.E10-08-0738). [PubMed: 21209316]

97. Consortium TU, UniProt: the Universal Protein Knowledgebase in 2023. Nucleic Acids Research 51, D523–D531 (2022)10.1093/nar/gkac1052%JNucleicAcidsResearch).

98. Needleman SB, Wunsch CD, A general method applicable to the search for similarities in the amino acid sequence of two proteins. Journal of molecular biology 48, 443–453 (1970); published online EpubMar (10.1016/0022-2836(70)90057-4). [PubMed: 5420325]

99. Abagyan RA, Batalov S, Do aligned sequences share the same fold? Journal of molecular biology 273, 355–368 (1997); published online EpubOct 17 (10.1006/jmbi.1997.1287). [PubMed: 9367768]

100. Stephens BS, Ngo T, Kufareva I, Handel TM, Functional anatomy of the full-length CXCR4-CXCL12 complex systematically dissected by quantitative model-guided mutagenesis. 13, eaay5024 (2020)doi:10.1126/scisignal.aay5024).

101. Keenan TM, Folch A, Biomolecular gradients in cell culture systems. Lab on a chip 8, 34–57 (2008); published online EpubJan (10.1039/b711887b). [PubMed: 18094760]

102. Coleman DE, Sprang SR, Crystal structures of the G protein Gi alpha 1 complexed with GDP and Mg2+: a crystallographic titration experiment. Biochemistry 37, 14376–14385 (1998); published online EpubOct 13 (10.1021/bi9810306). [PubMed: 9772163]

103. Mixon MB, Lee E, Coleman DE, Berghuis AM, Gilman AG, Sprang SR, Tertiary and quaternary structural changes in Gi alpha 1 induced by GTP hydrolysis. Science 270, 954–960 (1995); published online EpubNov 10 (10.1126/science.270.5238.954). [PubMed: 7481799]

104. Wall MA, Coleman DE, Lee E, Iniguez-Lluhi JA, Posner BA, Gilman AG, Sprang SR, The structure of the G protein heterotrimer Gi alpha 1 beta 1 gamma 2. Cell 83, 1047–1058 (1995); published online EpubDec 15 (10.1016/0092-8674(95)90220-1). [PubMed: 8521505]

105. Coleman DE, Berghuis AM, Lee E, Linder ME, Gilman AG, Sprang SR, Structures of active conformations of Gi alpha 1 and the mechanism of GTP hydrolysis. Science 265, 1405–1412 (1994); published online EpubSep 2 (10.1126/science.8073283). [PubMed: 8073283]

106. Longo PA, Kavran JM, Kim M-S, Leahy DJ, in Methods in Enzymology, Lorsch J, Ed. (Academic Press, 2013), vol. 529, pp. 227–240. [PubMed: 24011049]

107. Stephens BS, Ngo T, Kufareva I, Handel TM, Functional anatomy of the full-length CXCR4-CXCL12 complex systematically dissected by quantitative model-guided mutagenesis. Science signaling 13, (2020); published online EpubJul 14 (10.1126/scisignal.aay5024).

108. DeGraff JL, Gurevich VV, Benovic JL, The Third Intracellular Loop of α2-Adrenergic Receptors Determines Subtype Specificity of Arrestin Interaction *. Journal of Biological Chemistry 277, 43247–43252 (2002)10.1074/jbc.M207495200). [PubMed: 12205092]

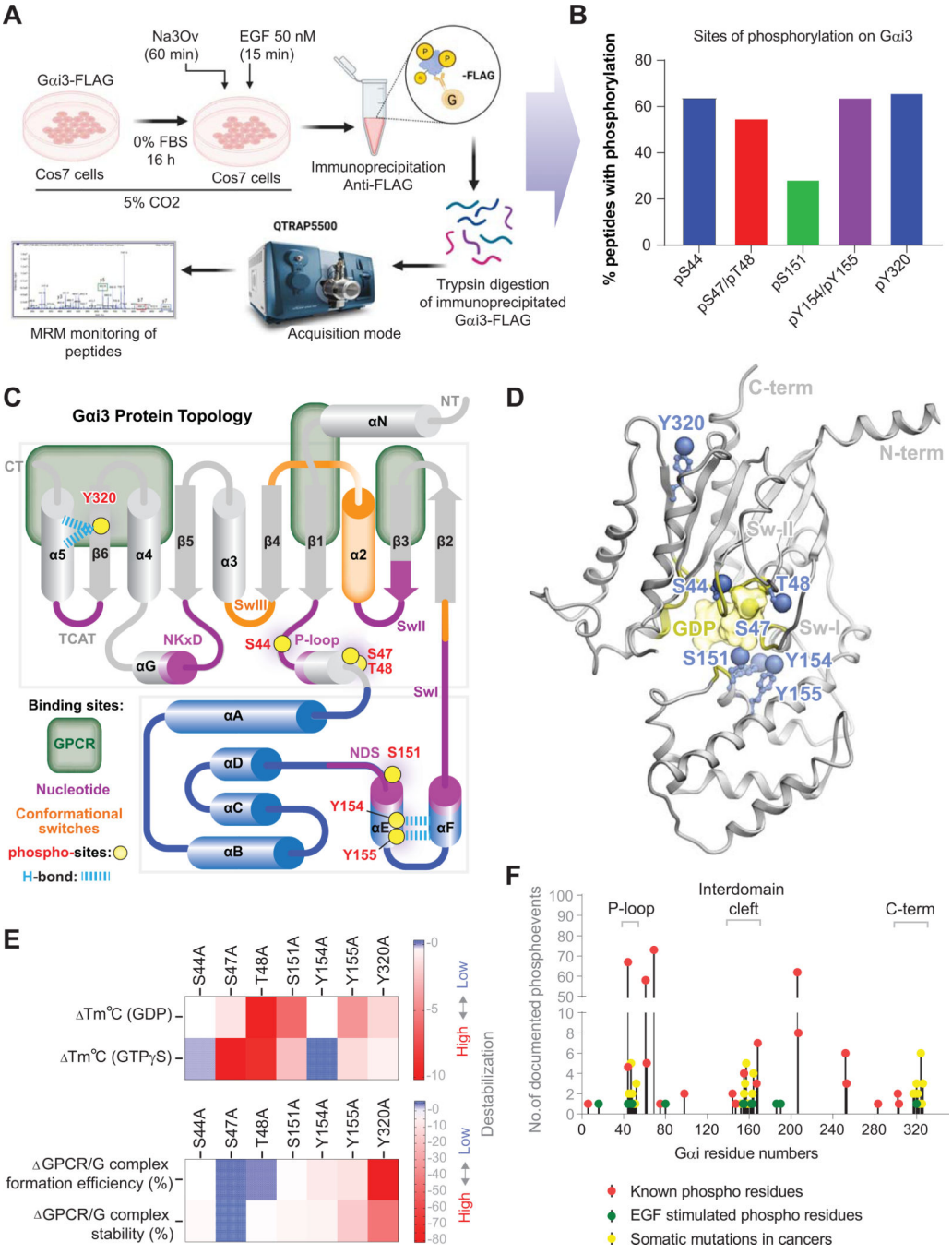

Fig. 1. Analysis of $G\alpha_{i3}$ phosphorylation in EGF-stimulated cells.

(**A**) Schematic of the experimental workflow used to discover phosphorylation events (phosphoevents) in $G\alpha_{i3}$ that occurred in cells stimulated with EGF. Serum-starved COS7 cells co-expressing untagged EGFR and C-terminally FLAG-tagged $G\alpha_{i3}$ were stimulated with 50 nM EGF. $G\alpha_{i3}$ immunoprecipitated from cell lysates with anti-FLAG mAb was digested on Protein-G beads and the tryptic fragments were analyzed by LC/MS without any further phosphoenrichment steps (see Materials and Methods). (**B**) The percentage of peptides containing the indicated phosphorylated residues on $G\alpha_{i3}$, which were calculated

as [phosphorylated peptides / total detected peptides] x 100. (**C** and **D**) Phosphosites on $G\alpha_{i3}$ that were identified by LC/MS in (A) and (B) are projected on a topology map of the $G\alpha_{i3}$ protein modified from Kalogriopoulos *et al.* (5) with conformational switches and binding sites of key interactors marked (C) and on a ribbon diagram of the solved crystal structure of $G\alpha_i$ (PDB: 5tdh). Residues indicated in red highlight phosphosites which were mutated to phosphomimic or nonphosphorylatable amino acid residues in this study. (**E**) Heatmaps display the experimentally determined changes in the thermal stability of Gαi1 and its ability to form complexes with GPCRs upon mutating key phosphosites [identified in (A) and (B)] to Ala(A), as reported previously (44). The thermal stability of each mutant is displayed (from top to bottom) in the inactive, GDP-bound and the active, GTP(GTPγS)-bound states, and the efficiency of formation (relative abundance) and relative stability of the reconstituted rhodopsin-G_i protein complex. Blue and red colors indicate low and high degrees of destabilization. For source data, see data file S3. (**F**) Lollipop diagram showing all documented serine, threonine, and tyrosine phosphorylation events on $G\alpha_{i1}$, $G\alpha_{i2}$, and $G\alpha_{i3}$, as well as somatic mutations in cancers. Red indicates data from phosphosite.org; green indicates experimental data from the current study; yellow indicates data from COSMIC (https://cancer.sanger.ac.uk/cosmic).

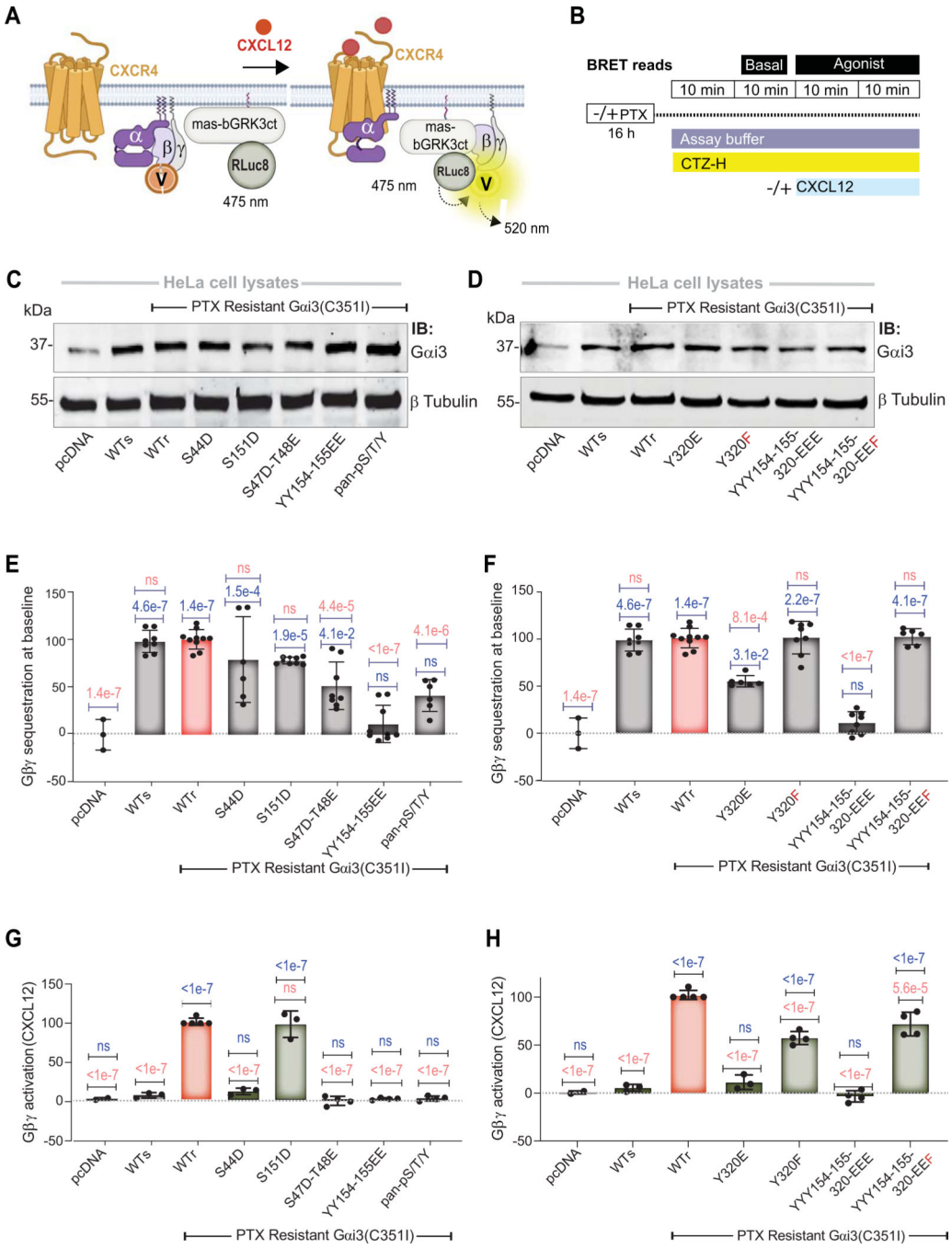

Fig. 2. Effects of phosphomimicking mutations in $G\alpha_{i3}$ on basal and CXCL12-stimulated activation of $G\beta\gamma$.

(**A** and **B**) Schematics of the principles (A) and the timeline for various treatments and readouts (B) of the BRET-based assay for assessing basal and ligand-stimulated $G\beta\gamma$ release from trimeric Gi. Before ligand stimulation (basal conditions), Venus-tagged $G\beta_1G\gamma_2$ complexes bind to $G\alpha_i$-GDP to form inactive trimers. Upon addition of 100 nM CXCL12, nucleotide exchange stimulates the release of Venus-$G\beta\gamma$ dimers from $G\alpha_i$, which enables them to bind to GRK3ct-RLuc8, resulting in an increase in the BRET signal. (**C** and **D**)

Western blotting analysis of the indicated phosphomimicking and non-phosphorylatable $G\alpha_i$ mutants in equal aliquots of HeLa cell lysates (~35 μg of total protein). β-Tubulin was used as a loading control. Western blots are representative of three independent experiments. (**E** and **F**) The percentage of Gβγ sequestration observed in cells expressing the indicated mutant under basal conditions, all analyzed under the same conditions as for (B), but in two sets as indicated. Results are expressed as the suppression of basal mVenus-Gβγ/GRK3ct-RLuc8 association normalized to a set scale of 0 to 100%, where 0% is in the absence of exogenous $G\alpha_i$ (pcDNA, negative control, no suppression) and 100% is in the presence of either PTX-sensitive (WTs) or PTX-resistant (WTr) $G\alpha_{i3}$ (positive controls, both maximally suppressing the basal mVenus-Gβγ/GRK3ct-RLuc8 BRET). All assays were performed in the presence of PTX. (G and H) The percentage Gβγ activation upon CXCL12 stimulation observed in cells expressing the indicated mutants (table S3), all analyzed under the same conditions as for (B), but in two sets as indicated. Results are expressed as the ligand-induced increase in mVenus-Gβγ/GRK3ct-RLuc8 association (indicative of Gβγ release from $G\alpha_i$ and resulting activation), and normalized observed to a set scale of 0 to 100%, where 0% is pcDNA and the PTX-sensitive $G\alpha_{i3}$ (WTs) (negative controls, unable to release and activate Gβγ in response to CXCL12 in PTX-treated conditions) and 100% is the PTX-resistant $G\alpha_{i3}$ (WTr, positive control, maximal release and activation of Gβγ in response to CXCL12 in PTX-treated conditions). *P* values were determined by one-way ANOVA with Tukey's multiple comparison's test. *P* values in blue and red fonts indicate statistical significance compared to the negative control (pcDNA/WTs) and positive control (WTr), respectively. Data are means ± SEM of four independent experiments, each with three technical replicates. In (E) and (F), PTX-treated and non-PTX treated samples from the same day were used as separate biological replicates; thus, data are from eight experiments, each with three technical replicates. See also fig. S3 for the composite data for all conditions.

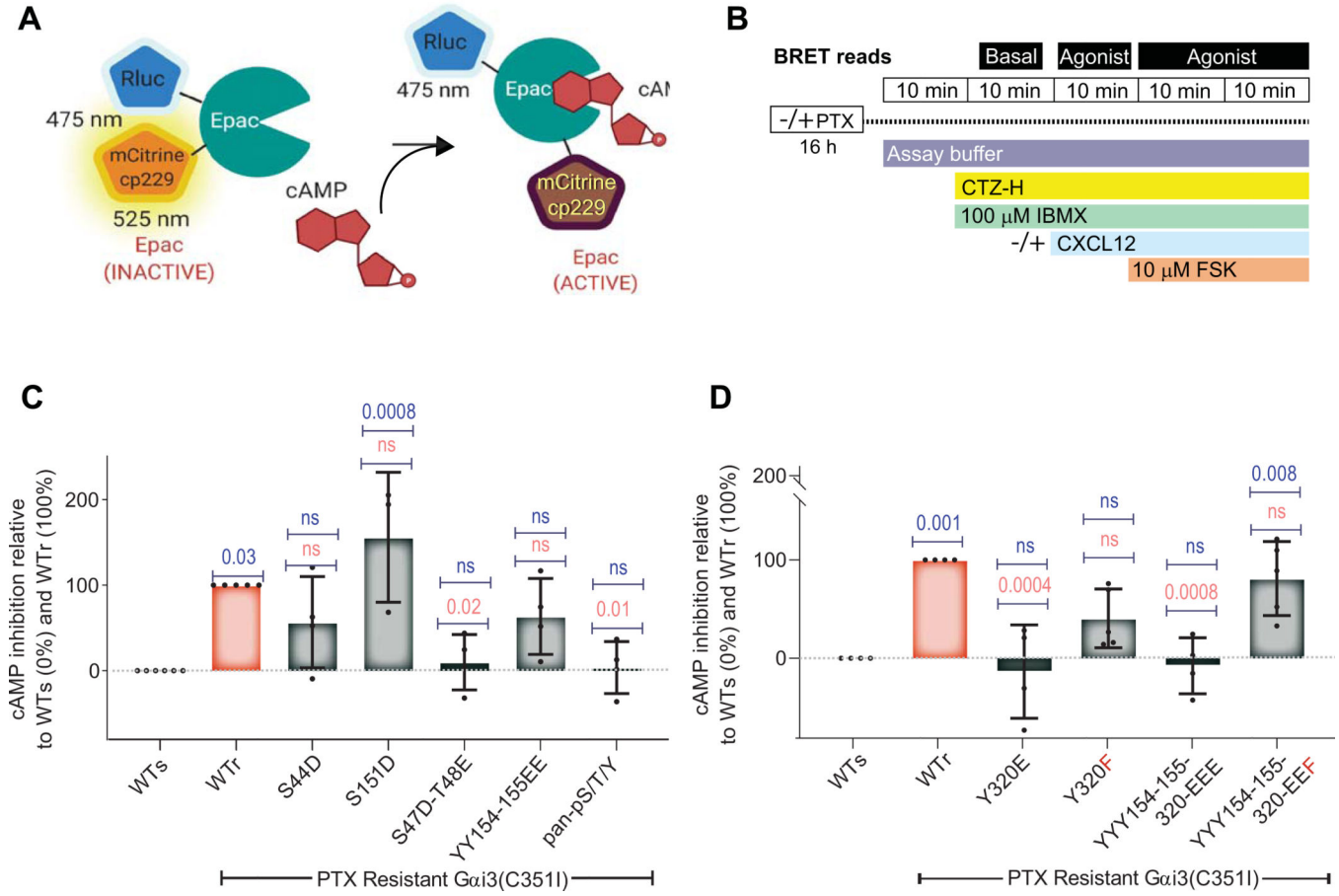

Fig. 3. Effects of phosphomimicking mutations in $G\alpha_{i3}$ on CXCL12-dependent inhibition of cAMP generation downstream of CXCR4.

(**A** and **B**) Schematics of the principle (A) and the timeline for various treatments and readouts (B) for the BRET-based CAMYEL assay for assessing the suppression of cAMP generation by WT and mutant $G\alpha_{i3}$. FSK was used to increase the concentration of cellular cAMP, which, upon binding to CAMYEL, decreases the BRET signal. Activation of $G\alpha_i$ reduces the extent of FSK-stimulated cAMP production, and consequently, increases the BRET signal. (**C** and **D**) The percentage of CXCL12-dependent inhibition of FSK-induced cAMP generation in HeLa cells transiently expressing the indicated $G\alpha_i$ variants and pre-treated with PTX. Results are normalized to a set scale of 0 to 100%, where 0% indicates cAMP inhibition mediated by the PTX-sensitive $G\alpha_{i3}$ in PTX-treated conditions (WTs, negative control, no inhibition of cAMP production) and 100% is the cAMP inhibition mediated by the PTX-resistant $G\alpha_{i3}$ (WTr, positive control, maximal inhibition of cAMP production). *P* values were determined by one-way ANOVA with Tukey's multiple comparison's test. *P* values in blue and red fonts indicate statistical significance compared to the negative control wild-type sensitive (WTs) and positive control resistant (WTr) G protein, respectively. Data are means ± SEM of four independent experiments, each with three technical replicates. See fig. S4A for the effect of each $G\alpha_{i3}$ mutant on basal, FSK-stimulated cellular cAMP amounts and see fig. S4B for each biological replicate.

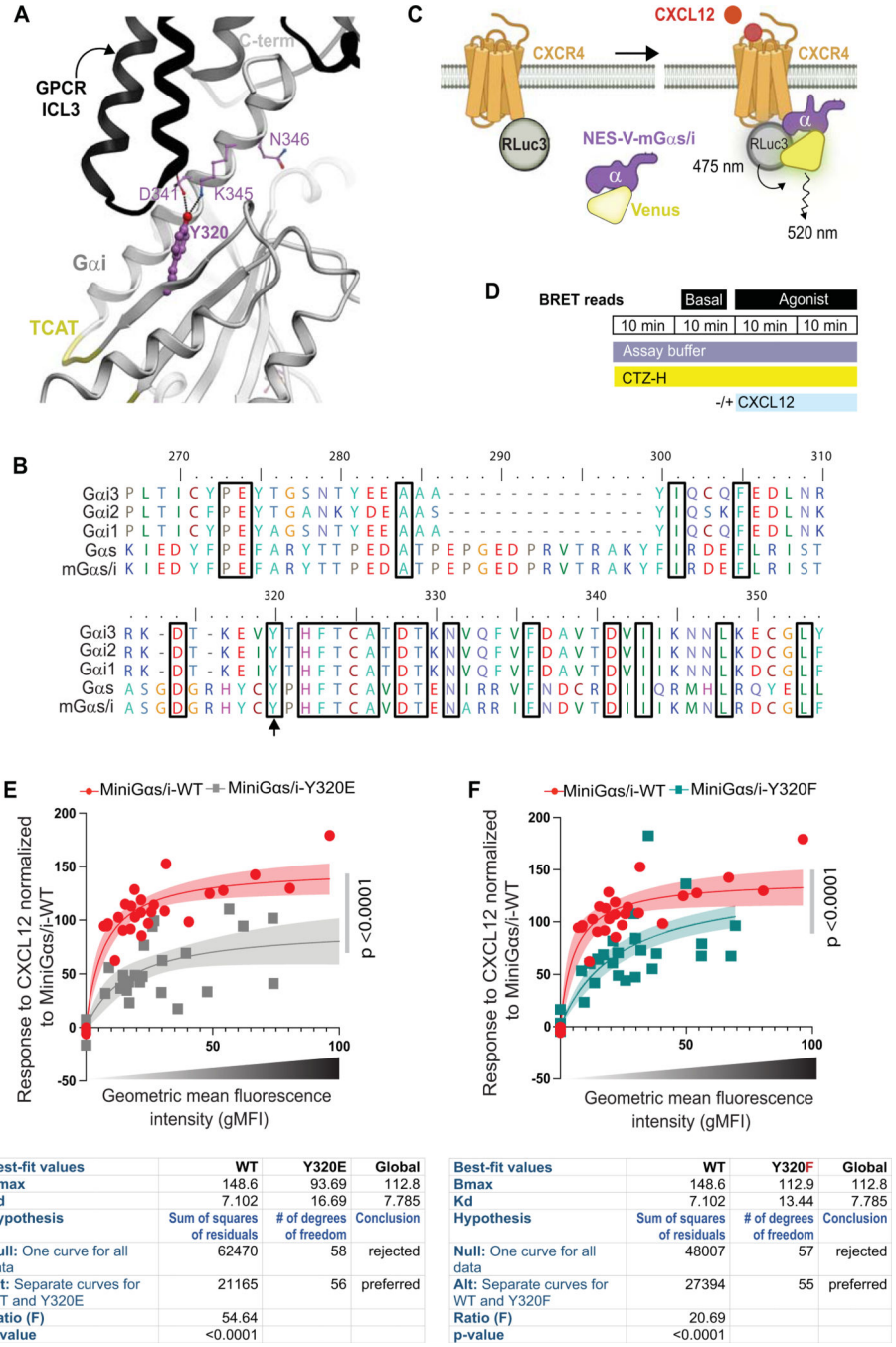

Best-fit values	WT	Y320E	Global
Bmax	148.6	93.69	112.8
Kd	7.102	16.69	7.785
Hypothesis	**Sum of squares of residuals**	**# of degrees of freedom**	**Conclusion**
Null: One curve for all data	62470	58	rejected
Alt: Separate curves for WT and Y320E	21165	56	preferred
Ratio (F)	54.64		
p-value	<0.0001		

Best-fit values	WT	Y320F	Global
Bmax	148.6	112.9	112.8
Kd	7.102	13.44	7.785
Hypothesis	**Sum of squares of residuals**	**# of degrees of freedom**	**Conclusion**
Null: One curve for all data	48007	57	rejected
Alt: Separate curves for WT and Y320F	27394	55	preferred
Ratio (F)	20.69		
p-value	<0.0001		

Fig. 4. Effects of phosphomimicking and nonphosphorylatable mutants of Tyr^{320} on the recruitment of GiPCRs to Gαi.

(**A**) Ribbon diagram of the solved crystal structure of a $G\alpha_i$-bound GPCR (PDB: 6cmo) highlighting the interaction surface of the GiPCR intracellular loop 3 (ICL3) with the C-terminal α5 helix of $G\alpha_i$. Residues crucial for the stabilization of the receptor-bound state are interactions between β6 (Tyr^{320}) and α5 (Asp^{341}, Lys^{345}, and Asn^{346}). (**B**) Alignment of the sequences of rat $G\alpha_{i1}$, $G\alpha_{i2}$, and $G\alpha_{i3}$ with Gαs and the mini-$G\alpha_{s/i}$ chimera used here. The arrow highlights Tyr^{320}. (**C** and **D**) Schematics of the principle

(C) and the timeline for the various treatments and readouts (D) of the BRET-based assay for assessing GPCR recruitment to the WT and mutant mini-$G\alpha_{s/i}$ chimeras. Proximity between the receptor (tagged with the BRET donor, RLuc3) and the mini-$G\alpha_{s/i}$ (tagged with the BRET acceptor, Venus) results in energy transfer (see Materials and Methods). (**E** and **F**) BRET-based saturation assays for mini-Gαs/i-WT vs, mini-Gαs/i-Y320E (E) and mini-Gαs/i-WT vs, mini-Gαs/i-Y320F (F) when a fixed amount of donor-encoding DNA (100 ng of CXCR4-RLuc3 per well in a 6-well plate) is co-transfected with increasing amounts of the acceptor-encoding DNA (mVenus mini-$G\alpha_{s/i}$ chimera; 0 to 2500 ng of DNA per well in a 6-well plate). The x axis indicates geometric mean fluorescence intensity (gMFI), whereas the y axis displays the CXCL12 response normalized to mini-$G\alpha_{s/i}$-WT (positive control). Data are from five independent experiments, each with four technical replicates. The semi-transparent bands associated with each fitting curve represent the range of the 95% confidence interval (CI). The F-test was performed to compute the significance of separate fits vs. global fit (see legend, table S5). According to the F-test, for both WT vs. Y320E and WT vs. Y320F, the null hypothesis (global fit) is rejected, with $P < 0.0001$. The Y320E Kd = 16.69, but the Y320F Kd = 13.44 compared to the WT Kd = 7.1; the Y320E Bmax = 93.69, but the Y320F Bmax = 112.9 compared to the WT Bmax = 148.6; E and F, table S5). Bar graphs showing the CXCL12 response (normalized to mini-$G\alpha_{s/i}$-WT), for the increasing amount of the acceptors, are presented in fig. S5A. Lineweaver-Burk (LB) plots (fig. S5, B and C). The slopes of the LB plots were significantly non-zero for mini-Gαs/i-WT and mini-Gαs/i-Y320F ($P = 0.0027$ and 0.0023, respectively), but not for mini-Gαs/i-Y320E [$P = 0.22$; (table S6)]. . Representative flow cytometry quantification for acceptor expression is shown in fig. S5, D to F. To calculate the Kd and Bmax values, data were fitted with a hyperbolic (one-site saturable binding) model in GraphPad Prism. For each pairwise comparison (mini-$G\alpha_{s/i}$-Y320E vs. mini-$G\alpha_{s/i}$ WT; mini-$G\alpha_{s/i}$-Y320F vs. mini-$G\alpha_{s/i}$ WT), an extra sum-of-squares F-test was performed to determine the significance of two separate construct-specific model fits vs. one global fit (see table S5).

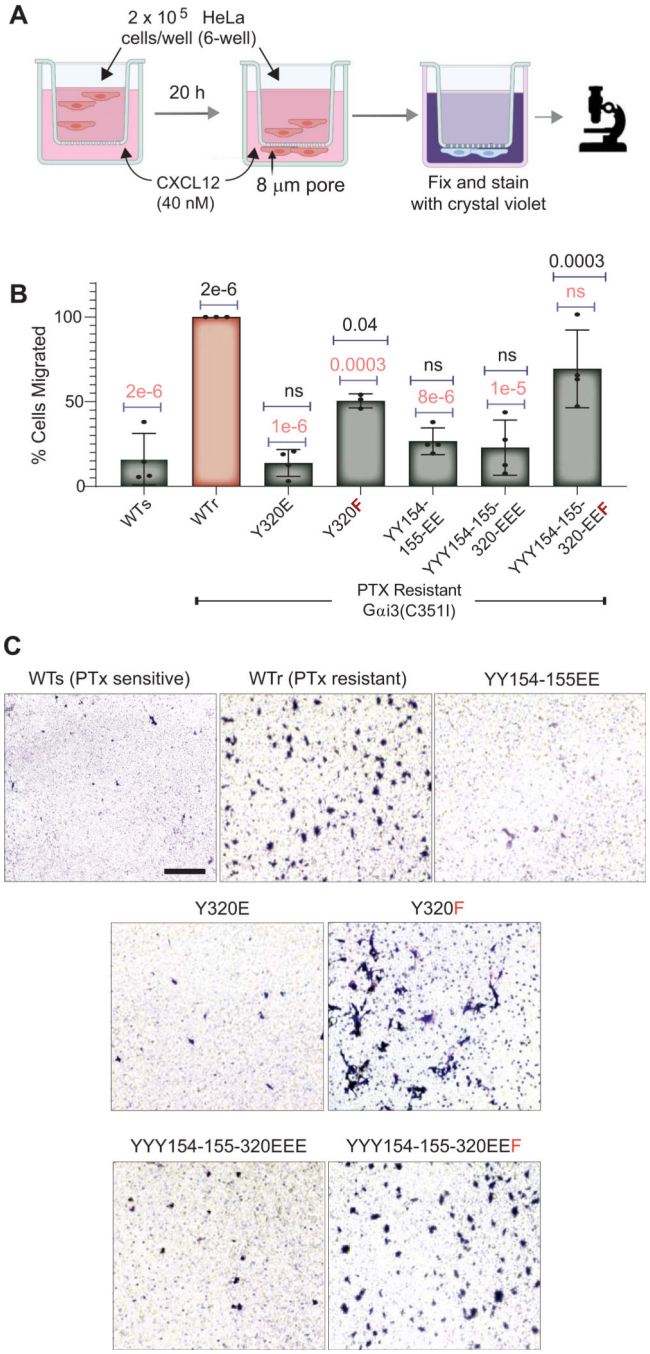

Fig. 5. A nonphosphorylatable mutant of Tyr^{320} in Gα_{i3} rescues CXCL12-stimulated chemotaxis.

(**A**) Schematic displays the pertinent details of a transwell cell migration assay to measure the chemotaxis of HeLa cells transiently expressing the indicated Gα_{i3} mutants across a 0 nM (top) to 40 nM (bottom chamber) CXCL12 gradient (see Materials and Methods). (**B**) Percentage cell migration compared to cells expressing the wild-type PTX-resistant (WTr positive control) Gα_{i3}. (**C**) Representative images of the crystal violet–stained transwell membrane shows cells that migrated along the CXCL12 gradient. Scale bar, 100 µm. *P*

values were determined by one-way ANOVA followed by Tukey's multiple comparison test. *P* values in black and red fonts indicate statistical significance compared to the negative control wild-type sensitive (WTs) and the positive control resistant (WTr) G proteins, respectively. Data are means ± SEM of three or four independent experiments, each with three technical replicates.

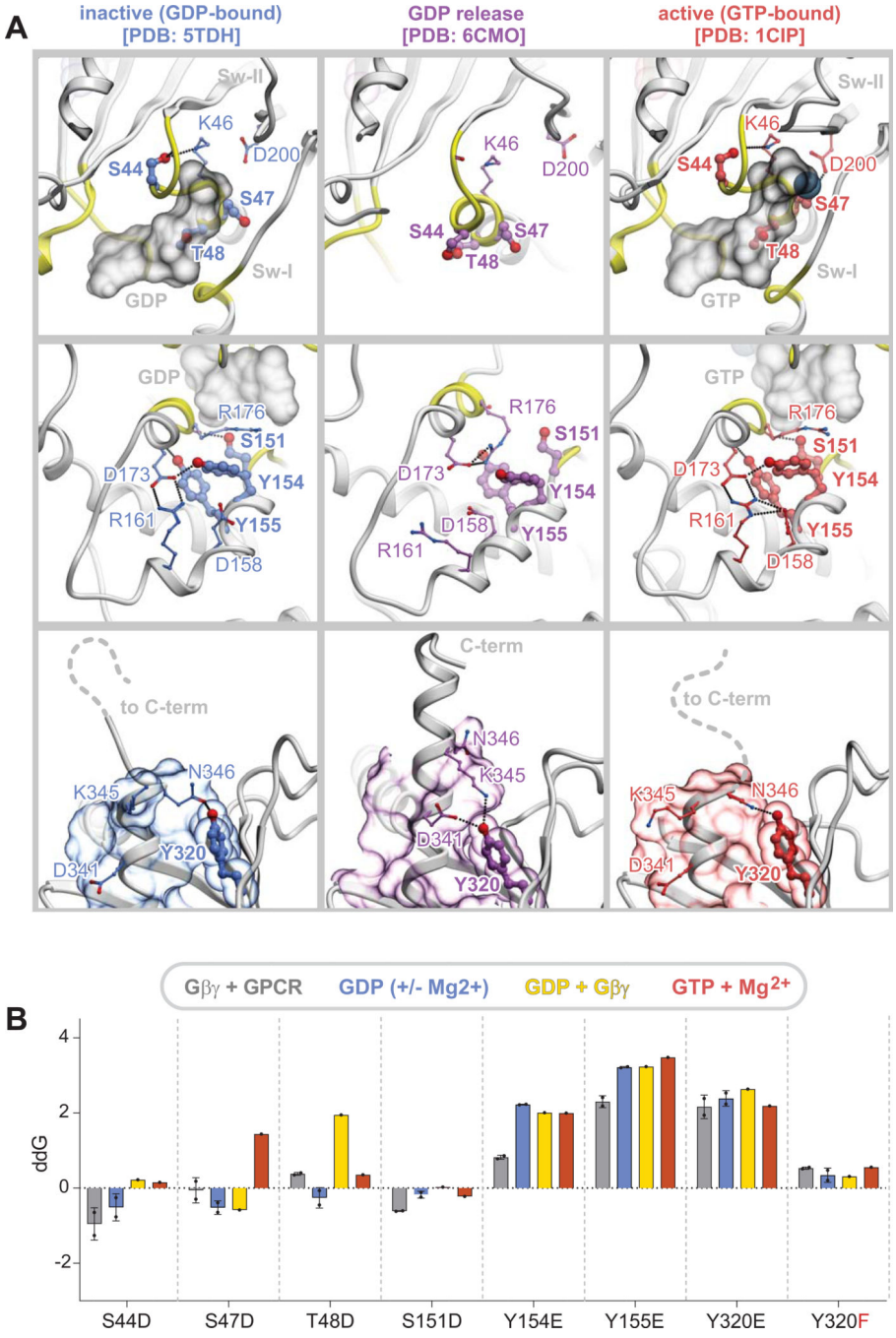

Fig. 6. Computational prediction of the effects of residue mutations on the stability of $G\alpha_i$ in various complexes.

(**A**) Crystal structure of WT $G\alpha_{i3}$, highlighting contact of the residues in the P-loop region (Top: Ser^{44}, Ser^{47}, and Thr^{48}), interdomain cleft (Middle: Tyr^{154} and Tyr^{155}), and the C-terminal α5 helix region packed against the β4 to β6 sheets (Bottom: Tyr^{320}), in their GDP- and Gβγ-bound inactive state (PDB: TDH), GDP release state (PDB: 6CMO), and GTP-bound active state (PDB:1CIP). H-bonds between the residues that were used in this study and their neighboring residues in the non-phosphorylated state. (**B**) Bar graph showing the

computationally predicted effects of phosphomimicking or nonphosphorylatable mutations on the stability of $G\alpha_{i3}$ in various complexes and conformations, including a complex with $G\beta\gamma$ and the GPCR (PDB:6cmo,6ot0), GDP (+/−Mg^{2+}; PDB:1bof, 1gdd), GDP and $G\beta\gamma$ (PDB:1gg2), GTP and Mg^{2+} (PDB:1gia). Bar height indicates ΔΔG, that is, the predicted change in the change in Gibbs free energy of folding; higher (more positive) bars reflect a larger degree of destabilization by the respective mutation, whereas negative numbers indicate the opposite. See fig. S6A for the relative stability of the different mutant state conformations and complex compositions compared to the $G\beta\gamma$-bound state, and fig. S6B for the extended analysis of both nonphosphorylatable substitutions (Ala, Phe) as well as phosphomimicking substitutions at each site.

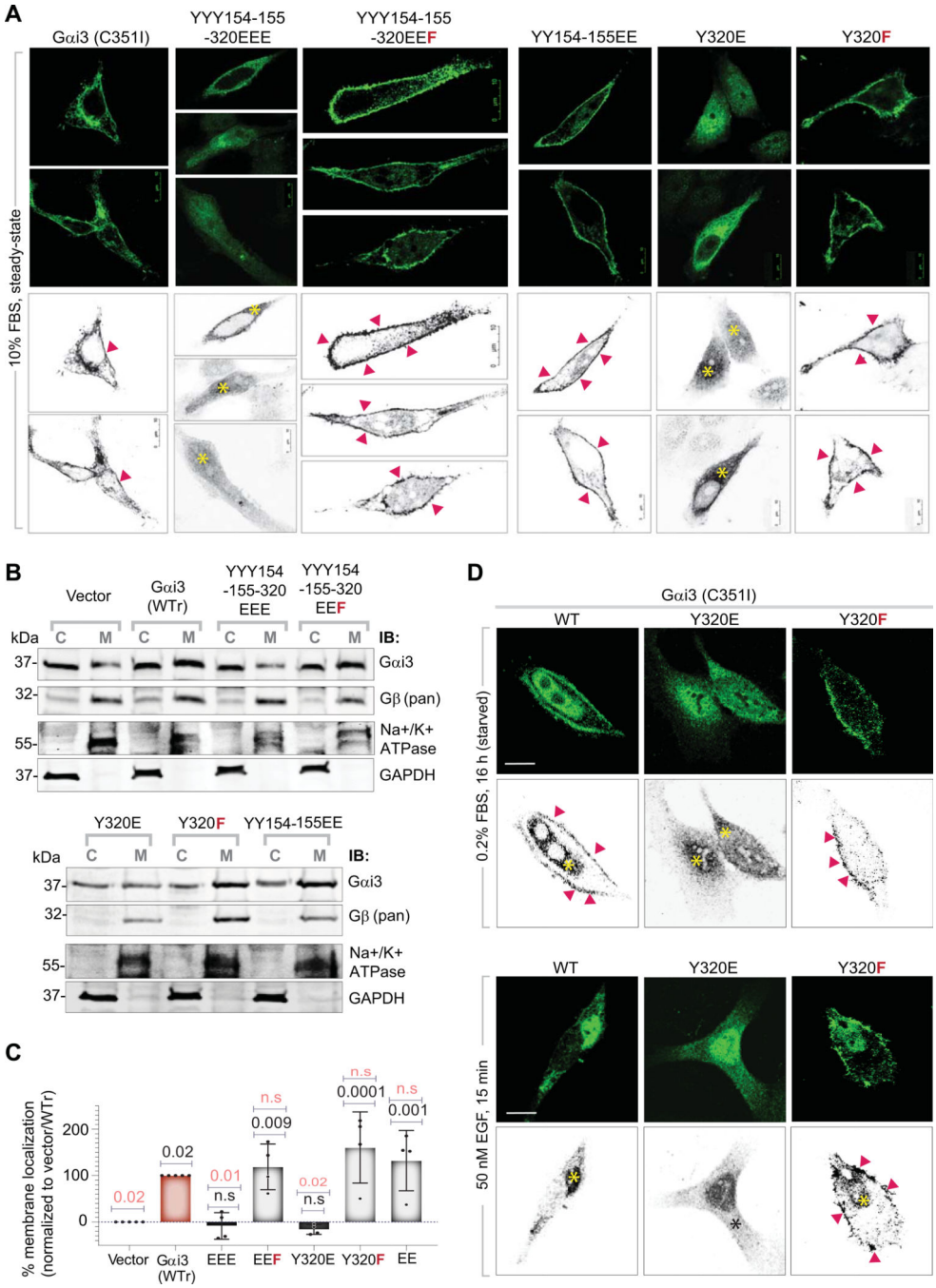

Fig. 7. Effects of phosphomimicking and nonphosphorylatable $G\alpha_{i3}$ mutants on protein localization.

(**A**) The subcellular localization of the indicated $G\alpha_{i3}$ constructs was assessed in transiently transfected HeLa cells by confocal immunofluorescence microscopy. Representative images are displayed as an assembled montage in (A). Top: green, $G\alpha_{i3}$. Bottom: green channels depicting $G\alpha_{i3}$ alone are presented in grayscale (red arrowheads indicate peripheral membrane localization; yellow asterisks indicate intracellular localization). Scale bars, 10 μm. (**B**) Membrane localization of the indicated $G\alpha_{i3}$ constructs and pan-Gβ were assessed

by subcellular fractionation of postnuclear supernatants derived from the homogenates of each transiently expressing HeLa cell line shown in (A). Western blots are representative of three independent biological replicates. C, cytosol; M, crude membranes. Cytosolic and membrane fractionations were assessed with the markers glyceraldehyde-3-phosphate dehydrogenase (GAPDH) and β1 sodium potassium ATPase (ATP1B1), respectively. (**C**) The Western blots in (B) were quantified by band densitometry and displayed as bar graphs. Results are expressed as a percentage of the distribution of $G\alpha_{i3}$ on membrane fractions on a set scale of 0 to 100%, where 0% is the vector alone (endogenous $G\alpha_{i3}$; negative control) and 100% is the PTX-resistant $G\alpha_{i3}$ (WTr, positive control). *P* values were determined by one-way ANOVA with Tukey's multiple comparison's test. *P* values in black and red fonts indicate significance compared to the negative control (vector) and the positive control (WTr) conditions, respectively. Data are means ± S.E.M of four independent experiments. (**D**). The subcellular localization of the indicated $G\alpha_{i3}$ constructs was assessed in transiently transfected HeLa cells treated with and without 50 nM EGF for 15 min and visualized by confocal immunofluorescence microscopy. Representative images are displayed as an assembled montage in (A). Top: green, $G\alpha_{i3}$). Bottom: green channels depicting $G\alpha_{i3}$ alone are presented in grayscale (red arrowheads indicate peripheral membrane localization, whereas asterisks indicate intracellular localization). Scale bar, 10 μm.

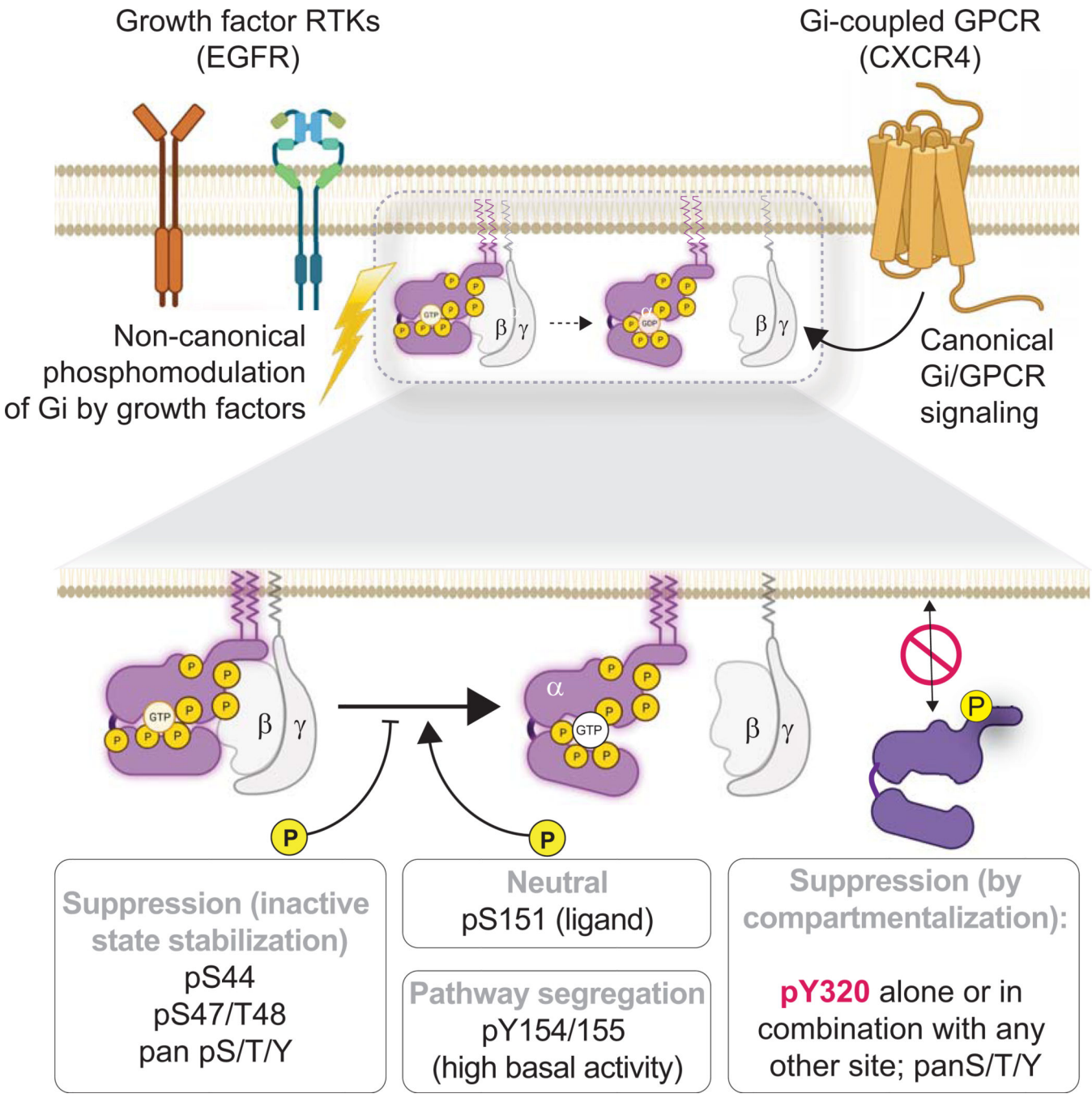

Fig. 8. Proposed effects of RTK-dependent Gα$_i$ phosphorylation on canonical GPCR signaling.

Growth factors may have at least three distinct effects on canonical signaling by Gi-coupled GPCRs through the phosphorylation of Gα$_i$ subunits. Phosphorylation of some clusters of amino acid residues may suppress signaling by stabilizing the GDP-bound conformation (Ser^{44}) or stabilizing the GDP/Gβγ-bound state (Ser^{47}/Thr^{48}) of Gα$_i$ and thereby impeding ligand-stimulated nucleotide exchange and trimer dissociation (Ser^{44}, Ser^{47}, and Thr^{48}). Phosphorylation at other sites may either have no effect (Ser^{151}) or result in segregation (Tyr^{154}, Tyr^{155}) between noncanonical (RTK-dependent) and canonical (GPCR-dependent)

pathways, while maintaining high basal activity due to defective Gβγ sequestration. Finally, phosphorylation at one key site (Tyr^{320}) may compartmentalize signaling through the regulation of G protein localization at the plasma membrane. See also table S8 for a comprehensive summary of all of the mutants tested in this study.

Table 1.

Phosphorylated sites within $G\alpha_{i3}$ that were identified by linear ion-trap mass spectrometry. The sites studied in this work are underlined.

Peptide sequence	Phosphorylated residue(s)
AAVERS[Pho]K	pS16
DGGVQAC[Cam]FS[Pho]R	pS141
SREYQLNDS[Pho]AAY[Pho]YLNDLDR	pS151 †
EYQLNDS[Pho]AAY[Pho]YLNDLDR	
RLWRDGGVQACFSRSREYQLNDS[Pho]ASY[Pho]YLNDLDR	
EYQLNDSASY[Pho]Y[Pho]LNDLDR	pY154 §* /pY155 §*
IS[Pho]QTNYIPTQQDVLR	pS163 *
LLLGAGES[Pho]GK	pS44 *§†
S[Pho]T[Pho]IVKQK	pS47 † /pT48 †
TTGIVET[Pho]HFTFKELYFK	pT187
TTGIVETHFT[Pho]FK	pT190
S[Pho]KMIDR	pS16
VVVYSNTIQS[Pho]IIAIIR	pS263
EVY[Pho]THFTC[Cam]ATDTK	pY320 *§‡

* Sites reported to be phosphorylated at phosphosite.org.

§ Sites previously reported to be phosphorylated in a ligand-dependent manner.

† Sites neighboring the nucleotide-binding pocket.

‡ Sites facing the GPCR-binding interface.